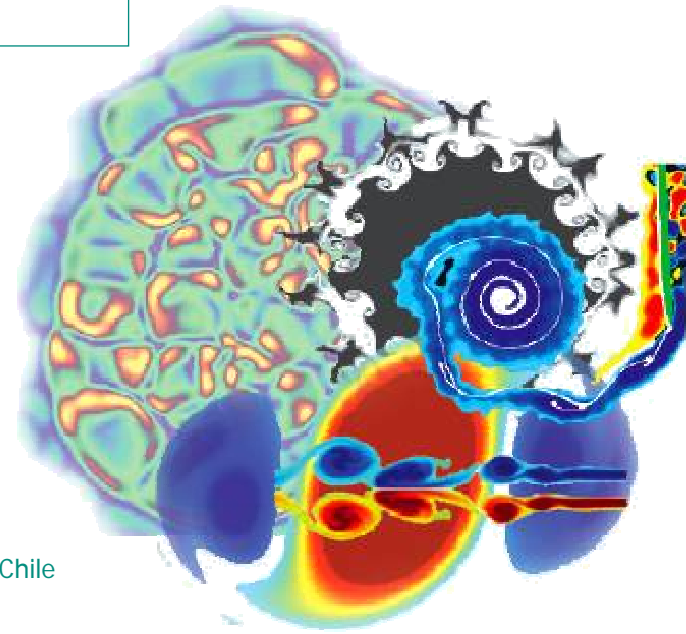


First Latin American SCAT Workshop:
Advanced Scientific Computing and Applications

Mixing, Droplets, Biomimetics, . .

Prof David Emerson
CCLRC Daresbury Laboratory
University of Strathclyde



Mixing

Fluid Dynamics: A Reminder of Some Key Parameters

Parameter	Symbol	Definition	Scale
Reynolds Number	Re	$\rho uL / \mu$	L
Knudsen Number	Kn	ℓ/L	1/L
Weber Number	We	$\rho u^2L / \sigma$	L
Capillary Number	Ca	$\mu u / \sigma$	-
Mach Number	M	u/c	-
Grashof Number	Gr	$g \rho^2 \beta (T_2 - T_1)L^3 / \mu^2$	L^3

Reynolds Number

Re < 2000

- Laminar flow
- Flow remains as distinct layers
- Physics relatively simple
- Mixing by diffusion
- Flow speed usually low

2000 < Re < 4000

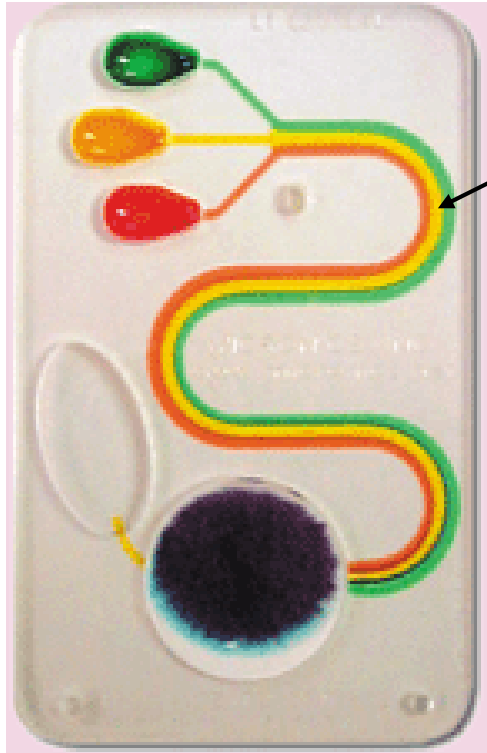
- Flow changing from laminar to turbulent
- Distinct layers are gone
- Physics quite complex
- Mixing by turbulence and diffusion
- Modest flow speeds

$$Re = \frac{\rho u L}{\mu}$$

Re > 4000

- Turbulent flow
- Flow chaotic: no distinct layers
- Physics very complex
- Mixing by turbulence
- Flow speed usually high

Microfluidics: laminar flow dominates!

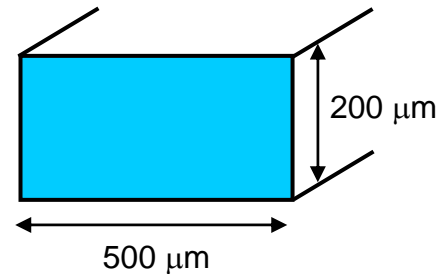


Laminar flow – very little mixing of the three coloured dyes.

An absorption-driven integrated microfluidic channel. The fluid is initially transported by surface tension and then flow is controlled by the absorption pad.

Consequences of scaling-down: laminar flow dominates

- Consider a rectangular etched micro-channel transporting water:



- Density, $\rho = 1000 \text{ kg/m}^3$; viscosity, $\mu = 10^{-3} \text{ Ns/m}^2$

F ($\mu\text{L}/\text{min}$)	F ($\mu\text{L}/\text{s}$)	U (mm/s)	Re
1	0.0166	0.166	0.033
1000	16.66	166.6	33.3

$$Re = \frac{\rho U D}{\mu}$$

Re \ll 2000 \Rightarrow laminar flow

NB: At 1 $\mu\text{L}/\text{min}$ it would take just over 1 year to pour a pint ($\sim 0.75\text{L}$)!

Consequences of scaling-down: mixing

- *In systems dominated by laminar flow:*
- mixing is only possible through diffusion
- diffusion requires time
- flow rates often too fast to allow sufficient time for complete diffusive mixing in short channels

d_{diff} = root-mean-square distance travelled by a molecule in time, t

$$d_{\text{diff}} = \sqrt{2Dt} \quad (\text{Einstein-Smoluchowski equation})$$

where, D = **diffusion coefficient** or “**diffusivity**” of the molecules (dependent on the temperature and molecular weight).

Typically $D = 10^{-9} \text{ m}^2/\text{s}$ for “small” molecules.

Example: for

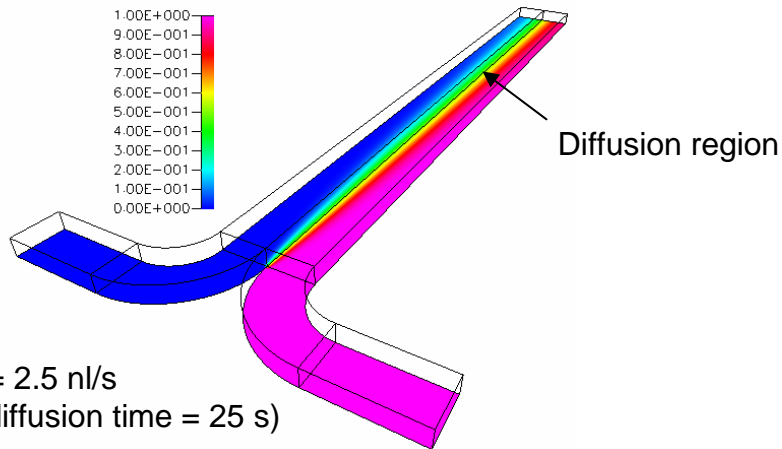
$t = 1 \text{ s} :$	$d_{\text{diff}} = 45 \text{ }\mu\text{m}$
$t = 2 \text{ s} :$	$d_{\text{diff}} = 63 \text{ }\mu\text{m}$
$t = 5 \text{ s} :$	$d_{\text{diff}} = 100 \text{ }\mu\text{m}$

Mixing - Diffusion

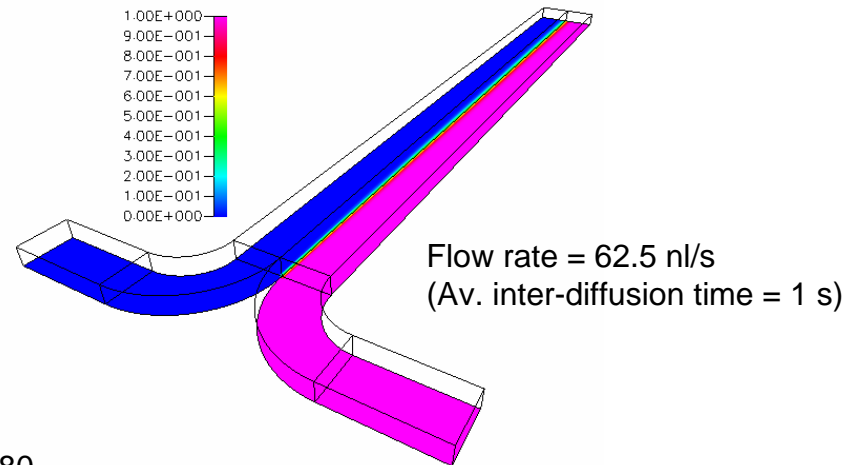
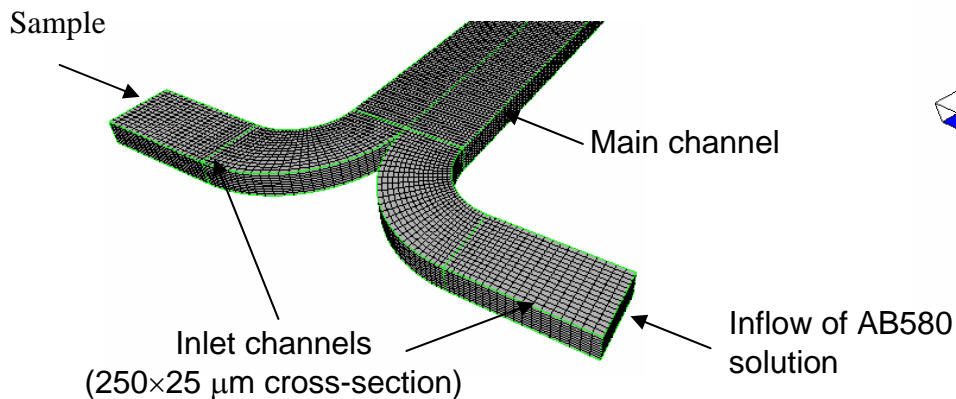
Diffusivity of physiologically important molecules suspended in water at 310K

Diffusing particle	Mol. Wt.	Diffusivity, D (m ² /s)
Glucose	180	7.1×10^{-10}
Sucrose	342	5.4×10^{-10}
Sodium fluorescein	376	5.0×10^{-10}
Lipase	6,669	1.5×10^{-10}
Serum albumin	68,460	6.5×10^{-11}
β -Lipoprotein	2,663,000	1.8×10^{-11}
Ribosome	4,000,000	1.3×10^{-11}
Tobacco mosaic virus	31,340,000	5.6×10^{-12}
T7 Bacteriophage	37,500,000	9.5×10^{-12}
1-micron spherical bead	$\sim 8 \times 10^{11}$	4.1×10^{-13}
Platelet ($\sim 2.4 \mu\text{m}$)	$\sim 4 \times 10^{12}$	1.6×10^{-13}
Yeast cell ($\sim 5.0 \mu\text{m}$)	$\sim 4 \times 10^{13}$	5.0×10^{-14}
Red blood cell ($\sim 5.6 \mu\text{m}$)	$\sim 6 \times 10^{13}$	6.8×10^{-14}

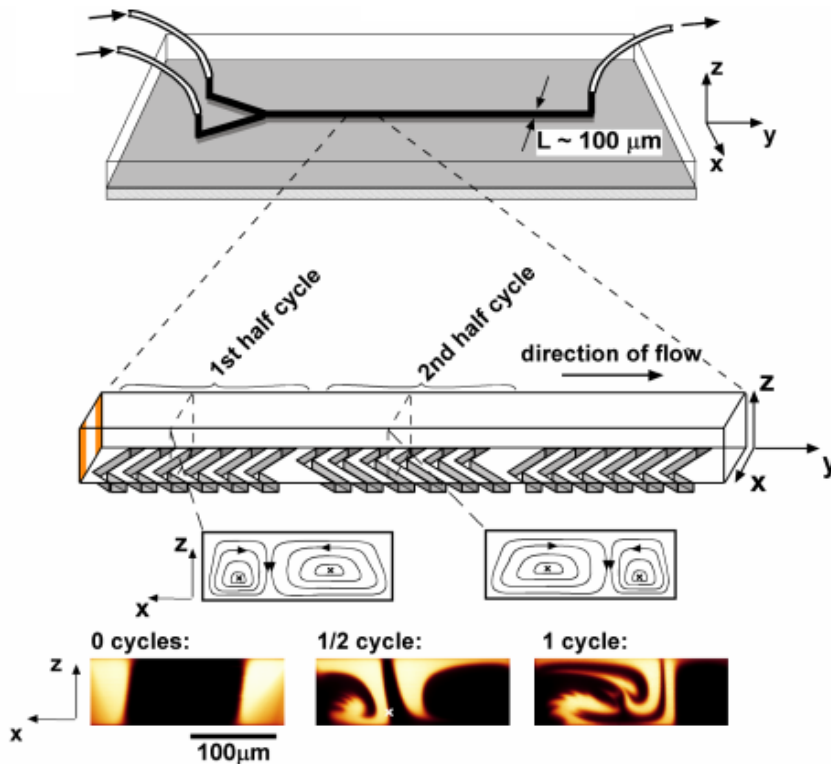
Mixing by diffusion requires time!



Diffusion of Albumin Blue 580 indicator dye (MW-306.8, diffusivity $4.55 \times 10^{-10} \text{ m}^2/\text{s}$) in a T-mixer

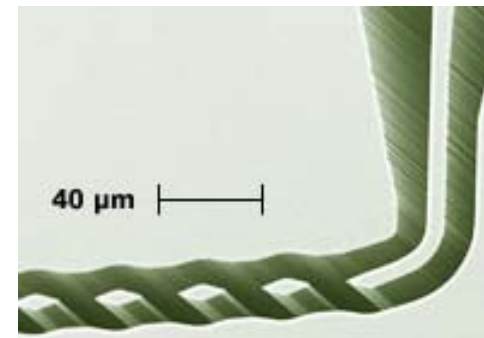
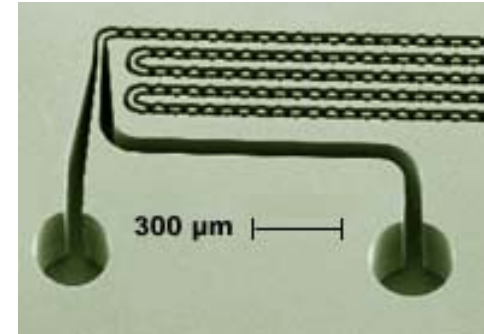


Strategies for improved mixing



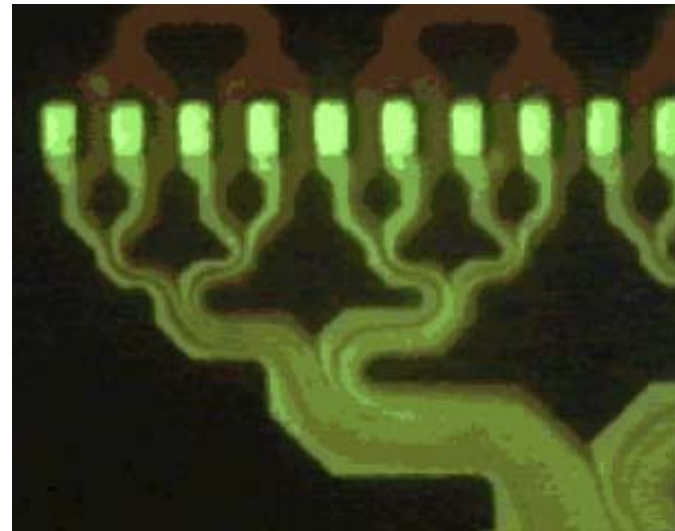
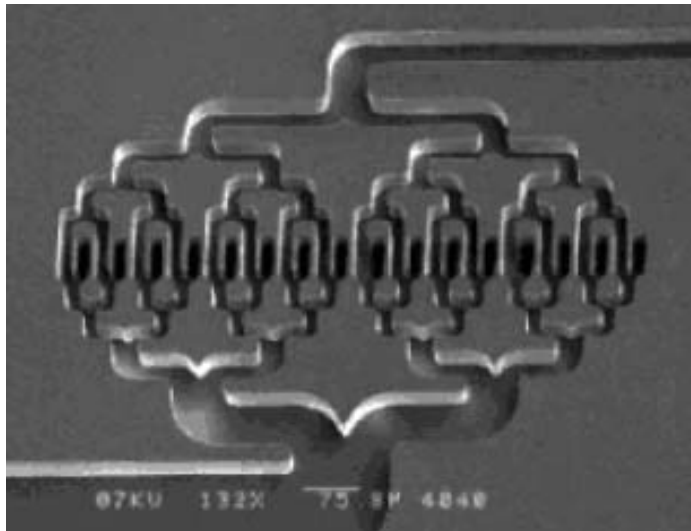
Staggered herringbone mixer

Ref. A.D. Stroock et al., "Chaotic mixer for microchannels"
Science, 2002, 295, 647-651.



Micro pillars
(200 μm high, 34 μm pitch)

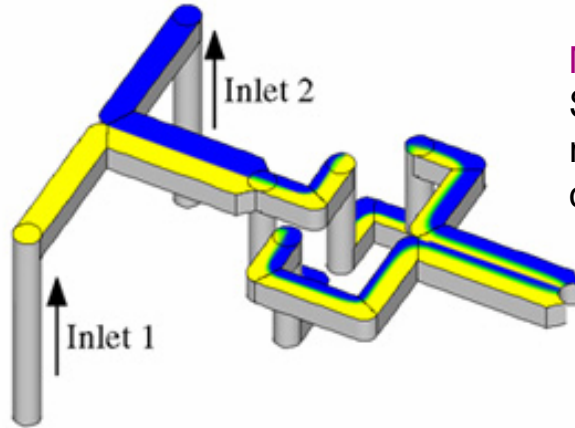
Strategies for improved mixing



Multilaminated glass-silicon micromixer
developed by Andreas Manz

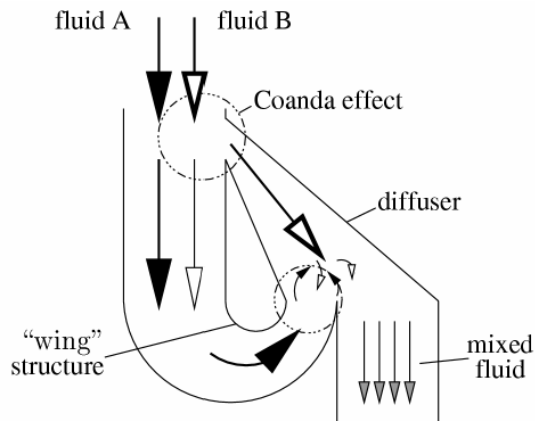
(32 microchannels each 20 μm wide)

More strategies for improved mixing!

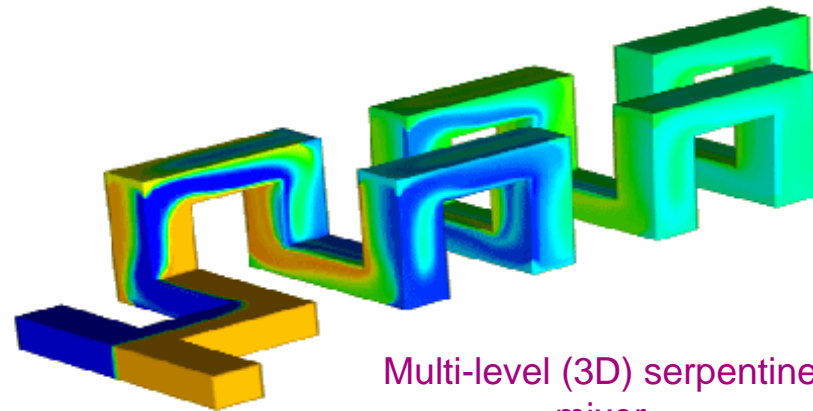


Multi-level (3D) laminating mixer

Successive vertical separation and horizontal reuniting of the fluid streams increases the contact area between the two fluids

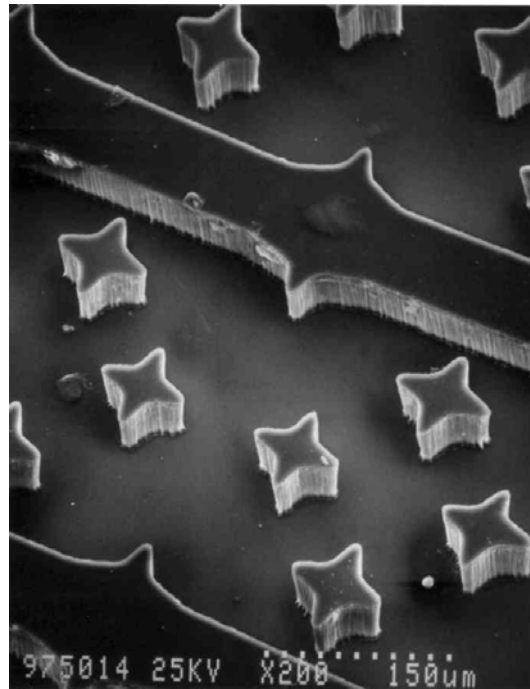
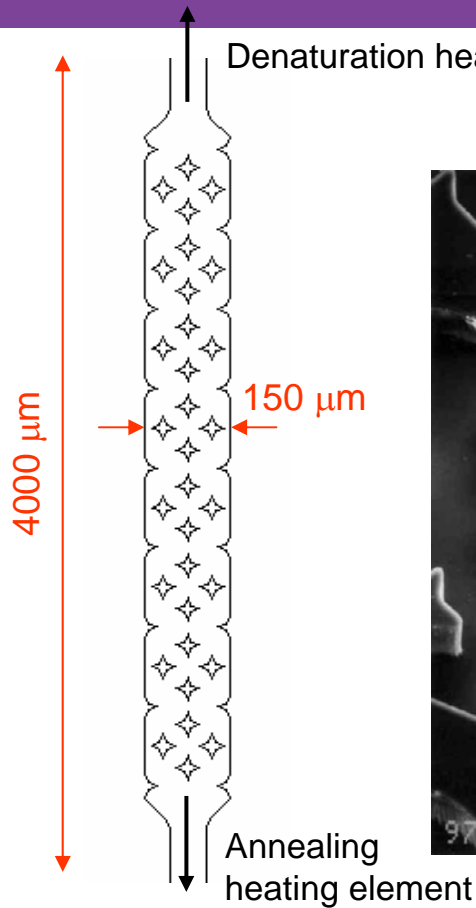


Coanda effect mixer



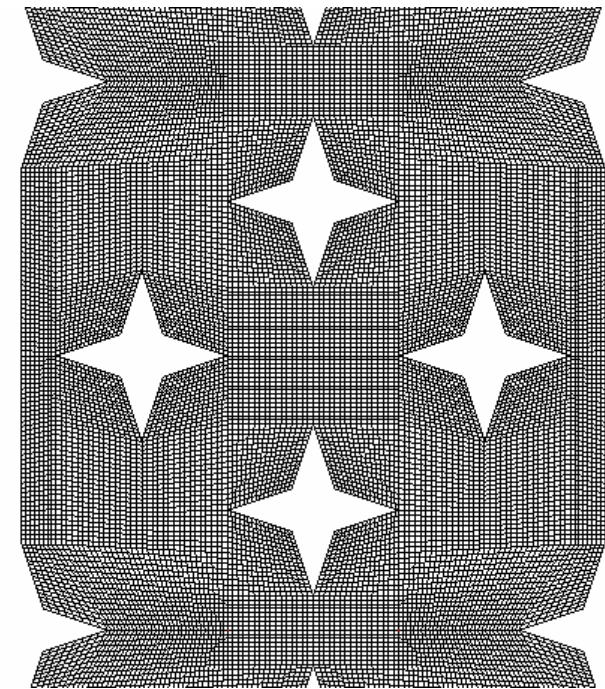
Multi-level (3D) serpentine mixer

Simulation of a novel multi-star PCR chip



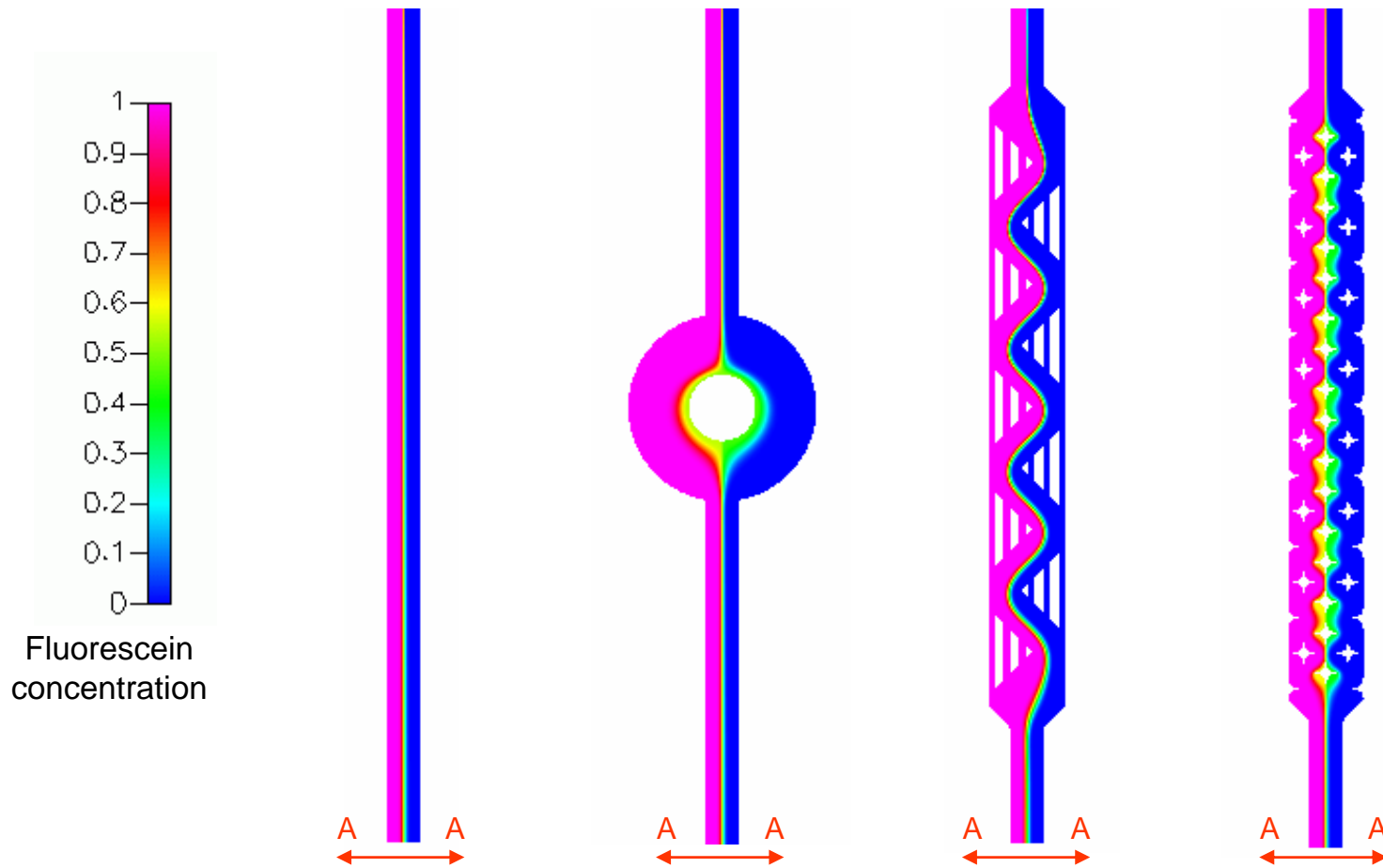
Scale drawing of
PCR mixer

SEM image of
micro-pillars

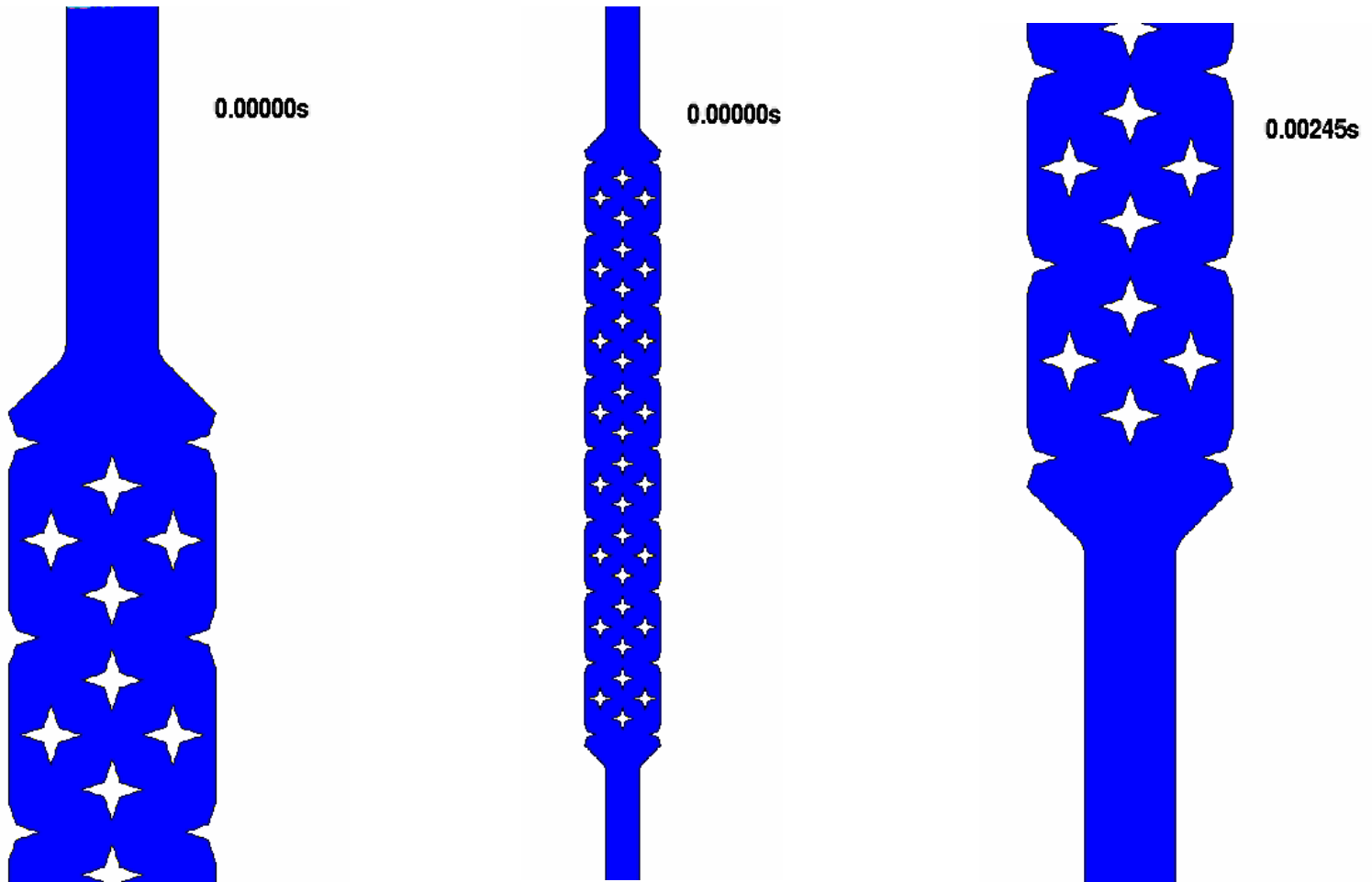


Detail of grid structure in central
region of mixing chamber

Comparison of chamber designs



Mixing for PCR



Vortex mixing - introduction

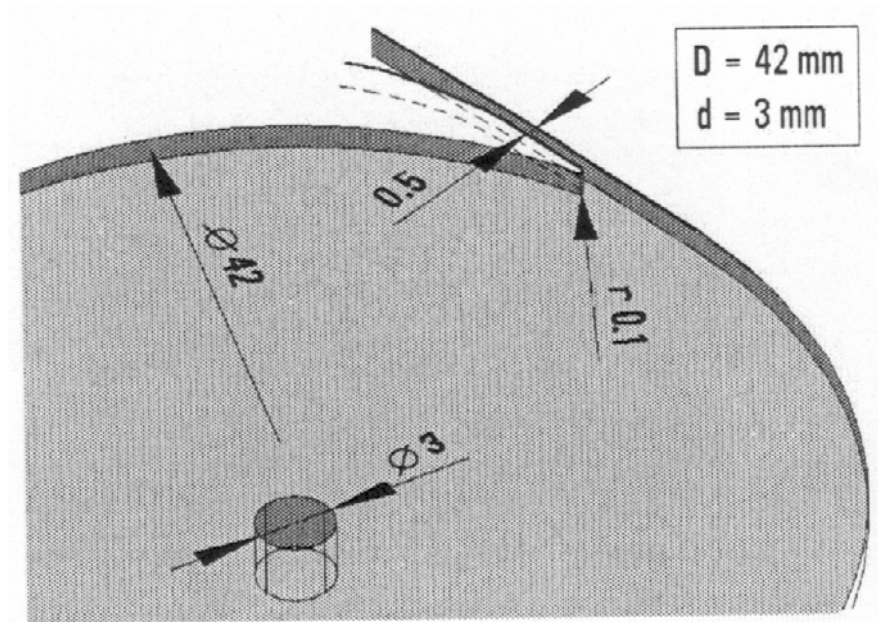
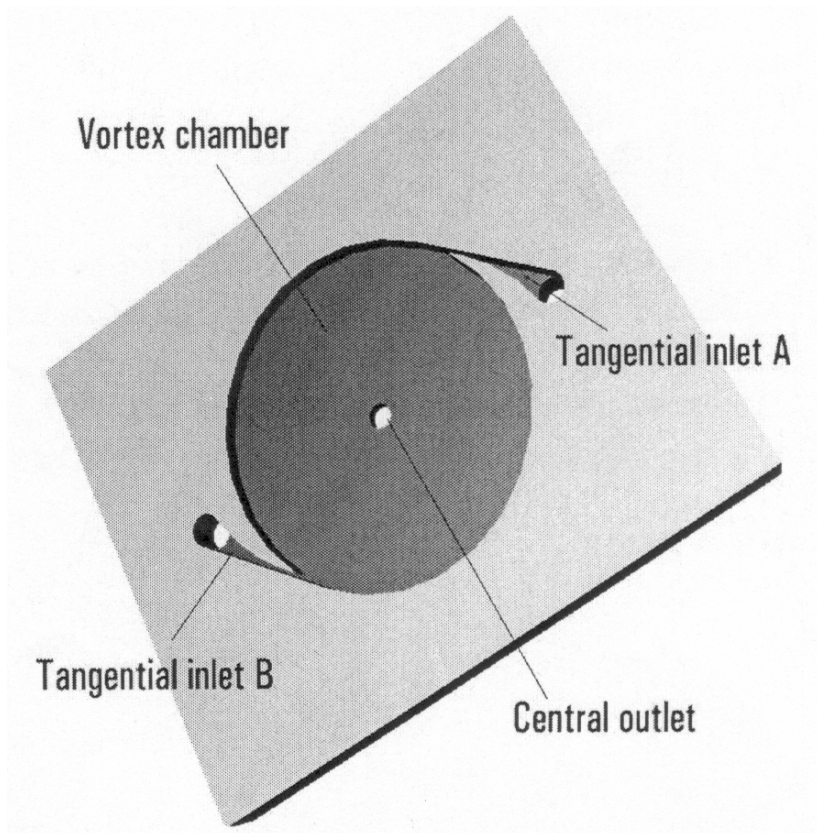
- Tesar and Low (2000)* state that “A shallow cylindrical cavity with *tangential* inlets for the two mixed fluids and a central outlet is a surprisingly effective mixer for operation at low Reynolds numbers (Re). However, the basic mechanism of adding thin successive layers to the rotating fluid ceases to be effective at very low Re, especially in shallow vortex chambers”.
- Problems with micro-mixers often arise due to the fact that the Reynolds number tends to be extremely low and it is therefore not possible to achieve efficient mixing via turbulent diffusion.
- Instead, microfluidic mixing devices have to rely upon *laminar (molecular-scale) diffusive transport processes* which are less efficient.

* Tesar, V. and Low, Y.Y. (2000), Proc. 9th Int. Symp. On Flow Visualisation, Carlomagno, G.M. and Grant, I. (Editors), paper no. 445.

Operating principles

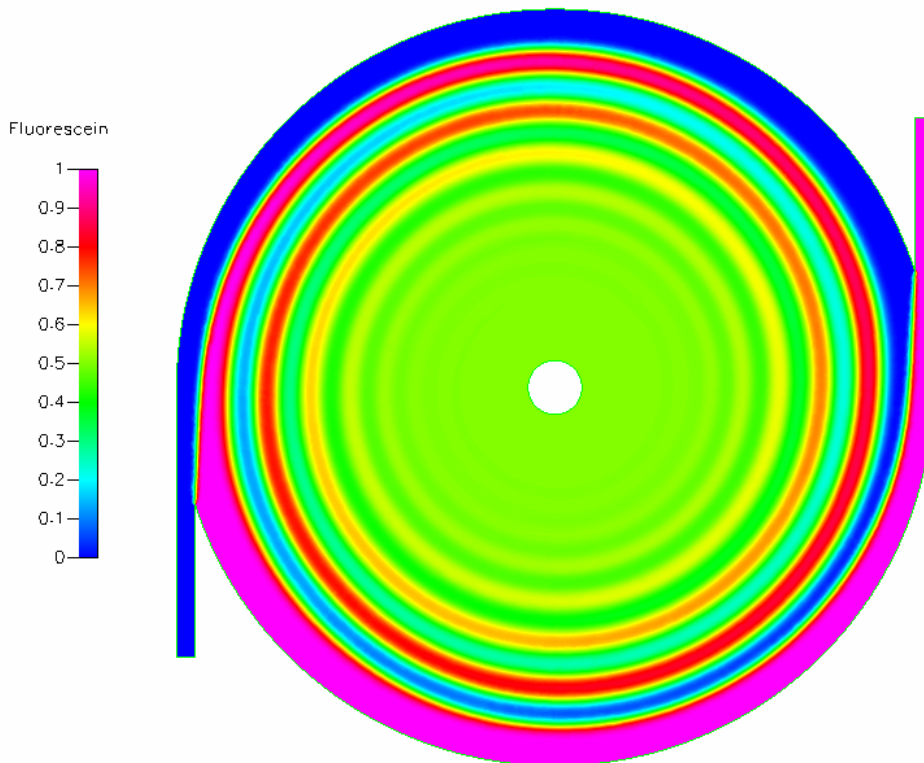
- To enhance the mixing by molecular diffusion, the essential feature of a micro-vortex mixer is to generate a repetitive structure of very thin interleaved laminae by successively adding fluid layers as the rotating flow passes each inlet nozzle in turn.
- Generation of an effective vortex mechanism requires a large ratio of chamber diameter (D) to exit diameter (d). (Preferably, this ratio should exceed 10).
- Ideally, the chamber height (h) should be large in relation to the chamber diameter (D). Unfortunately, this is often not possible with common micro-fabrication techniques (eg. etching).
- The small depth means that the fluid in the chamber is in closer contact with the relatively large areas of the flat top and bottom walls – this gives rise to large viscous forces between the fluid and the wall which tend to impede the rotational motion within the mixer.

Typical vortex mixer



Dimensions of a typical mixer with
2 tangential inlet nozzles

2D numerical simulation ($h/D = \infty$)



$Re_i = 100$

Summary of numerical model

$D = 42 \text{ mm}$; $d = 3 \text{ mm}$

87,858 unstructured (triangular) cells

$\rho = 1000 \text{ kgm}^{-3}$; $\mu = 10^{-3} \text{ Nsm}^{-2}$

Tracer: sodium fluorescein
(diffusivity = $4.55 \times 10^{-10} \text{ m}^2\text{s}^{-1}$)

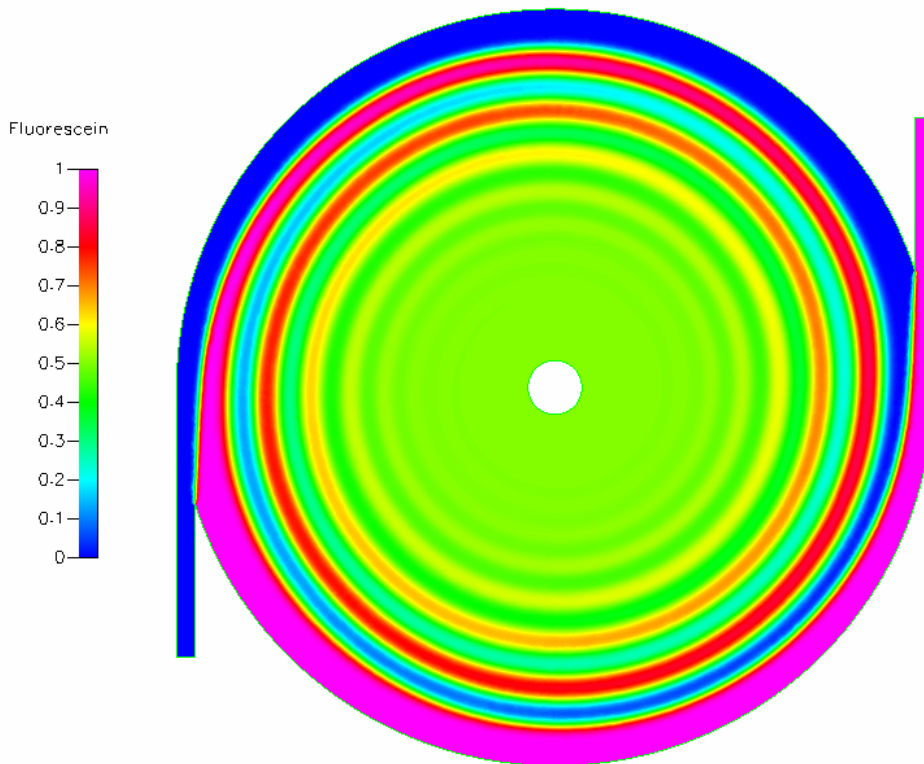
Average inlet velocity = 0.1 ms^{-1}

Inlet Reynolds number, $Re_i = 100$

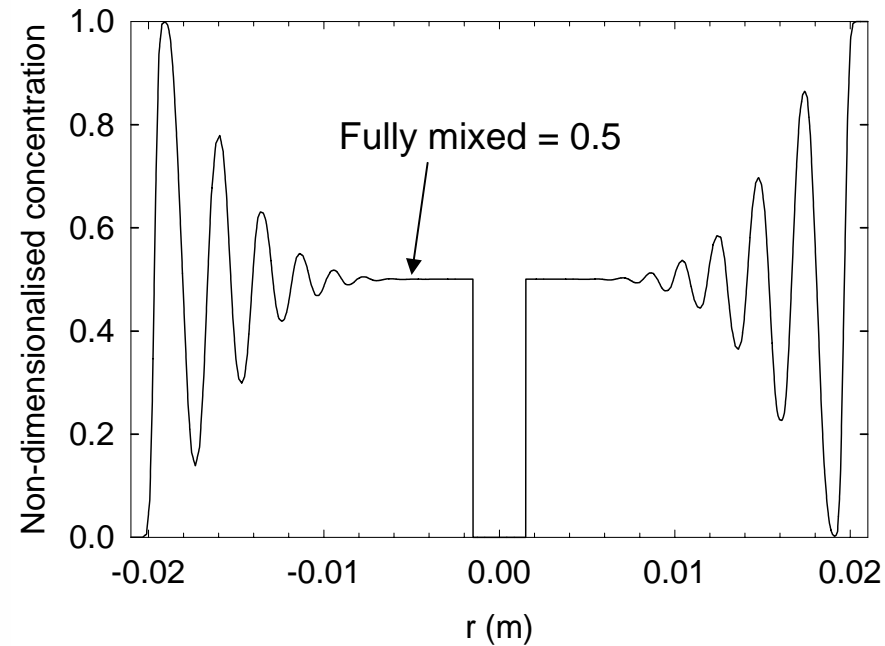
$$Re_i = \frac{\rho \bar{u}_i w_i}{\mu}$$

where w_i is the width of the inlet channel

2D numerical simulation ($h/D = \infty$)

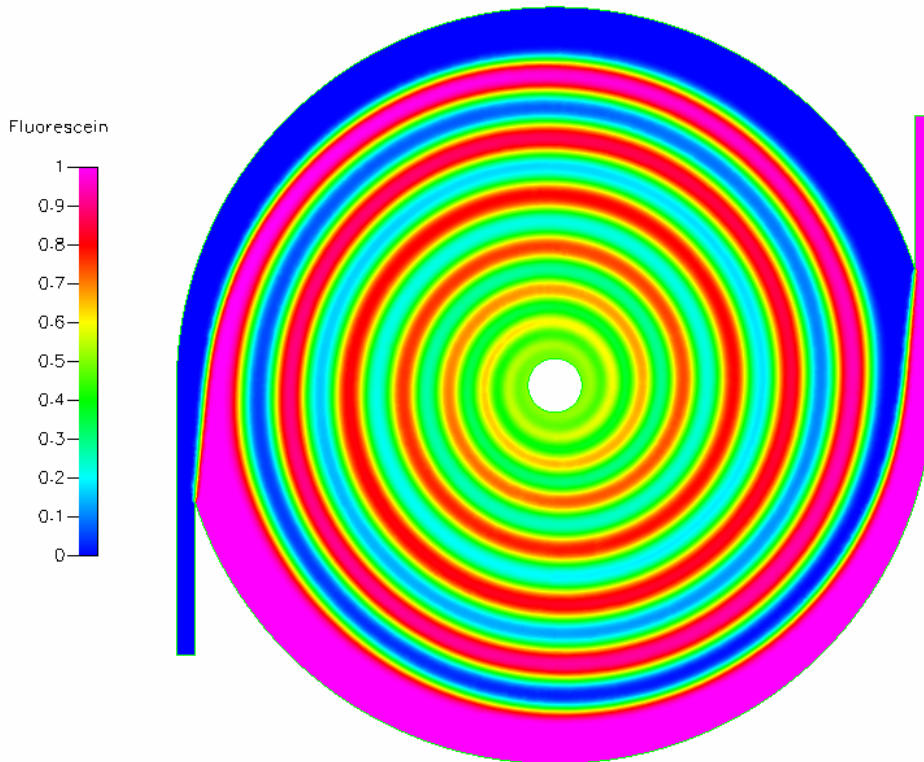


$Re_i = 100$

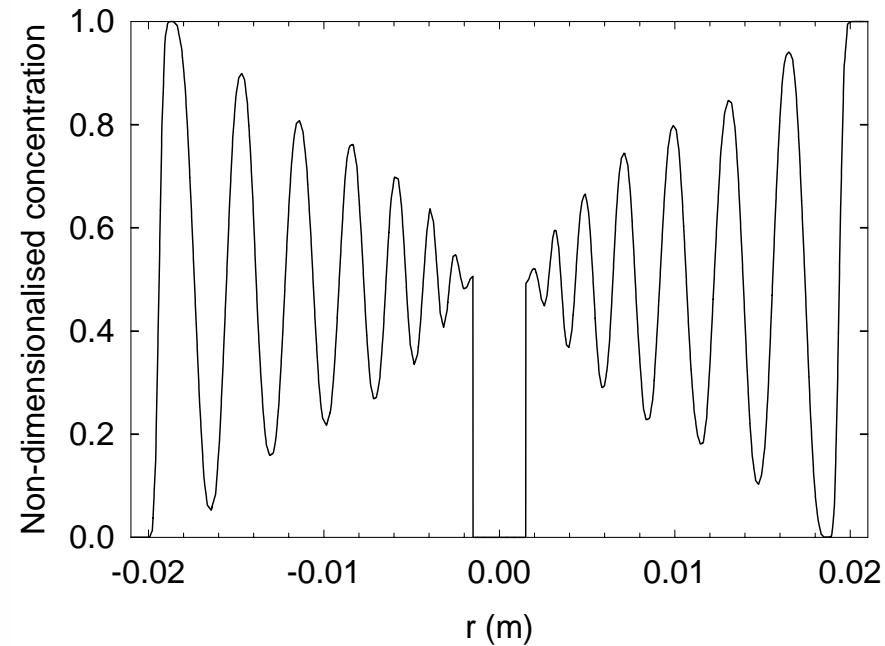


Distribution of sodium
fluorescein within vortex mixer

2D numerical simulation ($h/D = \infty$)

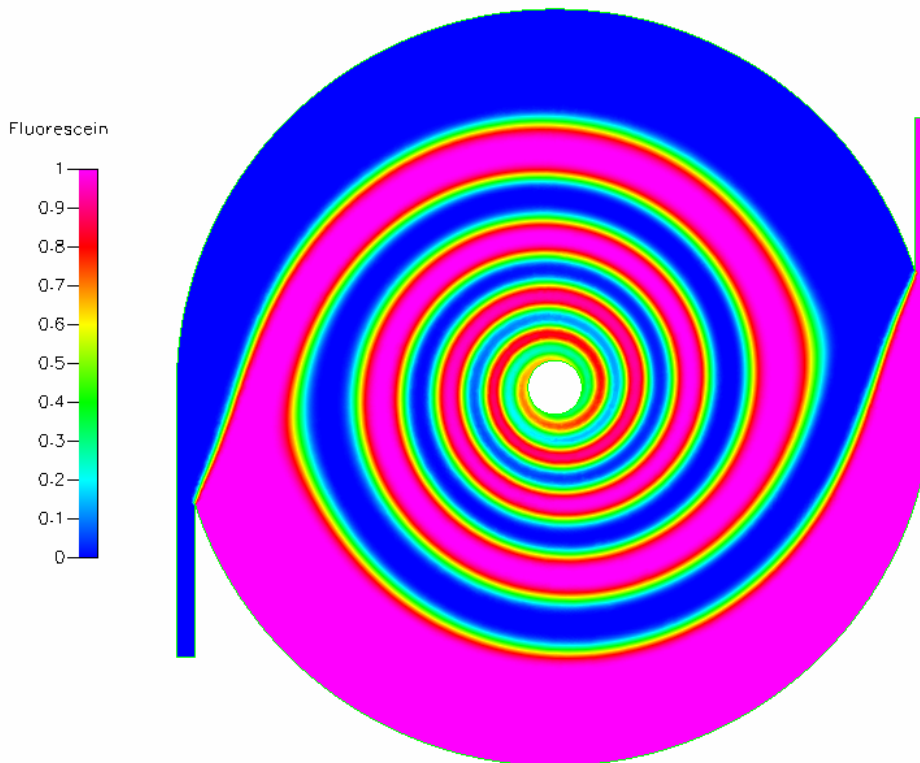


$Re_i = 50$

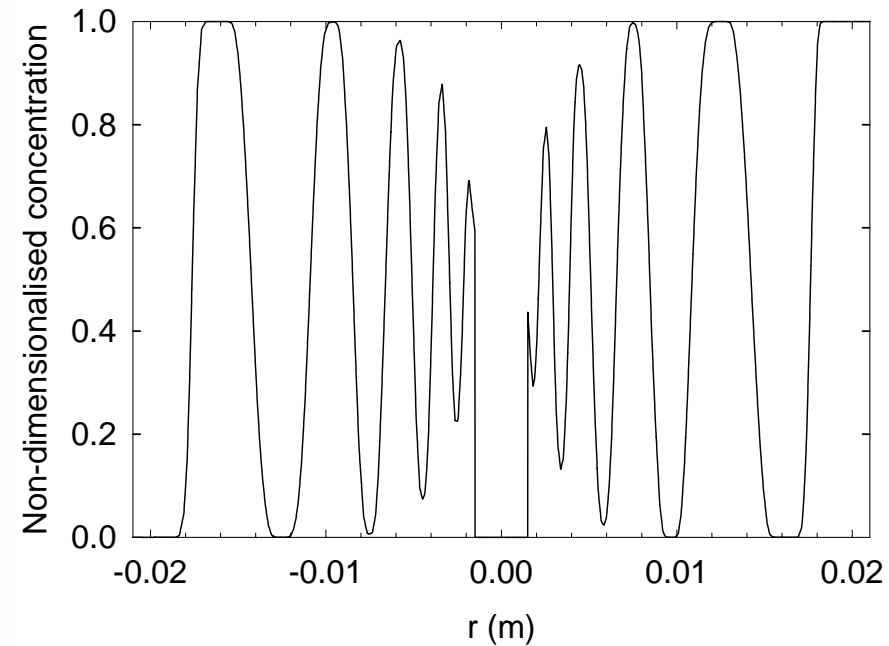


Distribution of sodium
fluorescein within vortex mixer

2D numerical simulation ($h/D = \infty$)

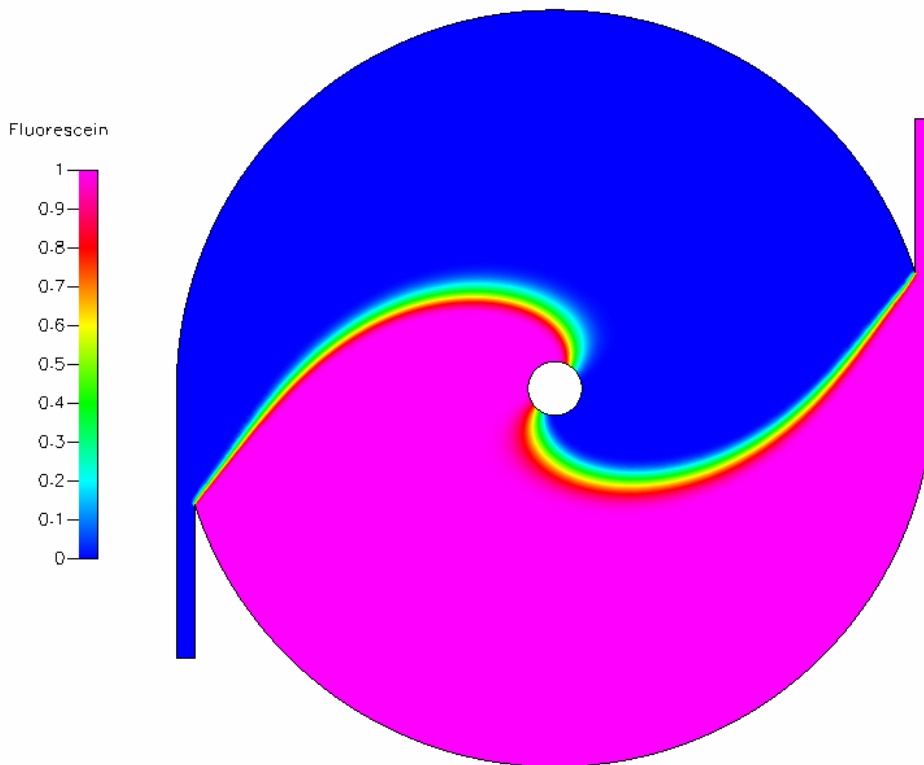


$Re_i = 10$

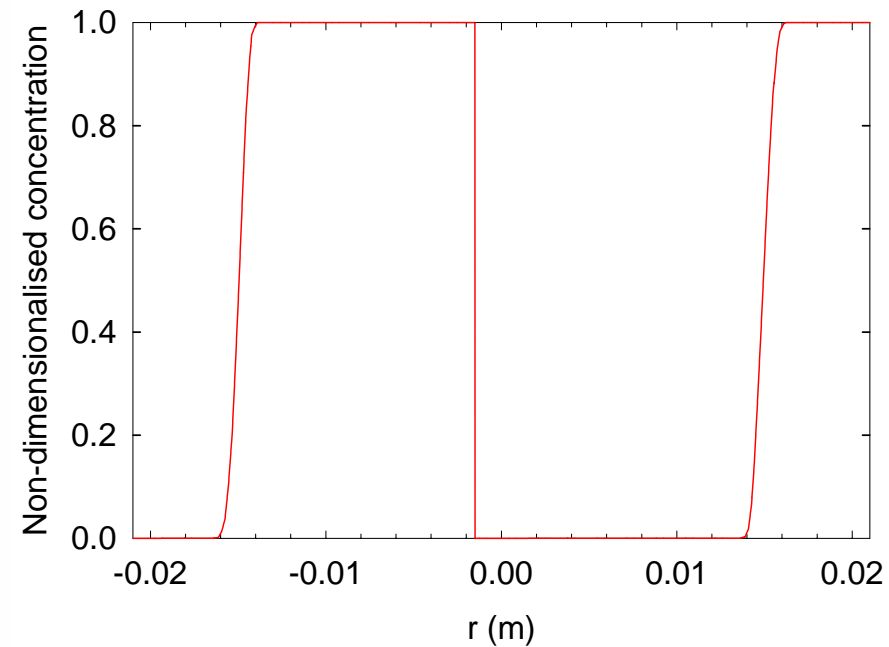


Distribution of sodium
fluorescein within vortex mixer

2D numerical simulation ($h/D = \infty$)

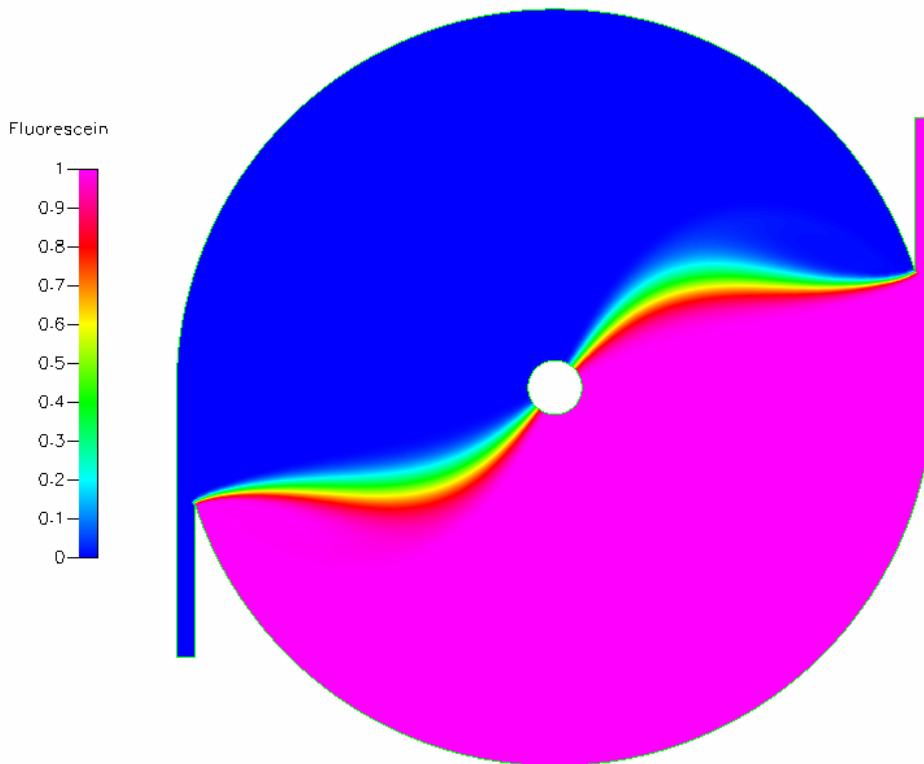


$Re_i = 5$

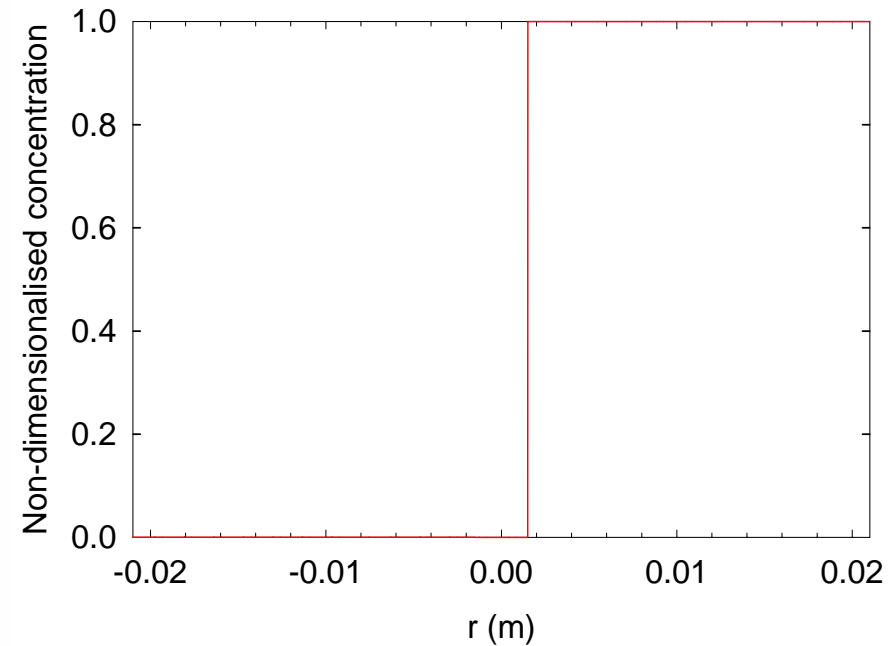


Distribution of sodium
fluorescein within vortex mixer

2D numerical simulation ($h/D = \infty$)



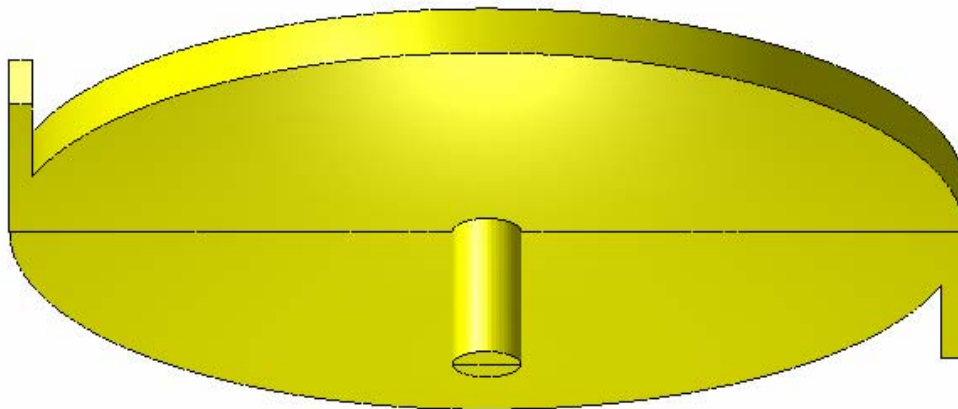
$Re_i = 1$



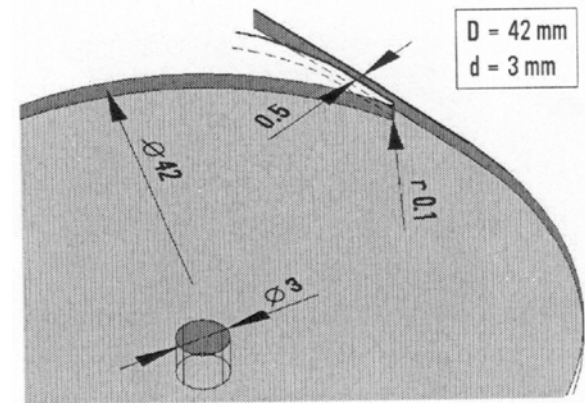
Distribution of sodium
fluorescein within vortex mixer

Effect of decreasing Reynolds number

- The results show that at high Reynolds numbers, thin interleaved layers are formed around the perimeter of the vortex chamber – leading to efficient mixing by diffusion as the flow progresses towards the central outlet.
- However, at low Reynolds numbers, increased internal fluid friction limits the effectiveness of the mixing and reduces the strength of the flow circulation.
- In addition, at low Reynolds numbers, the tangential motion imparted to the fluid in the chamber becomes negligible – and the fluid enters the chamber equally in all directions, despite the tangential inclination of the nozzles.



View from under mixer



Summary of numerical model

$D = 42 \text{ mm}$; $d = 3 \text{ mm}$; $h = 2.1 \text{ mm}$

675,550 triangular prismatic cells

$\rho = 1000 \text{ kgm}^{-3}$; $\mu = 10^{-3} \text{ Nsm}^{-2}$

Tracer: sodium fluorescein

(diffusivity = $4.55 \times 10^{-10} \text{ m}^2\text{s}^{-1}$)

Average inlet velocity = 0.5 ms^{-1}

Inlet Reynolds number, $Re_i = 500$

Droplets and surface tension

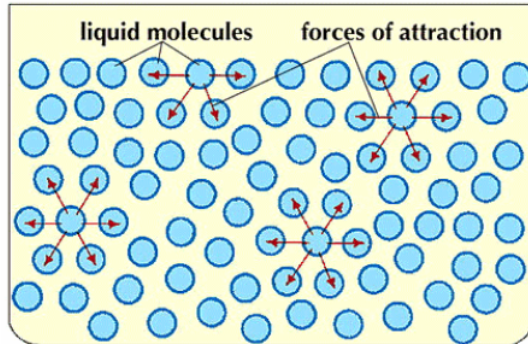
Consequences of scaling-down

- Surface tension becomes significant!



An adult water strider
(body length 10 mm)

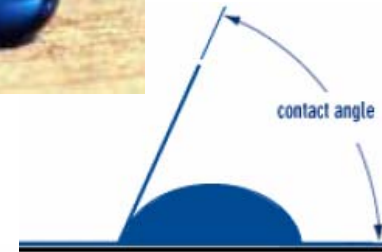
Surface tension



Surface tension - the intermolecular attractive forces at the surface of a liquid



$$\text{Capillary rise, } h = \frac{4\sigma \cos \theta}{\rho g d}$$



For water on a fully wetting surface:

$$\sigma = 0.073 \text{ Nm}^{-1} ; \theta = 0^\circ$$

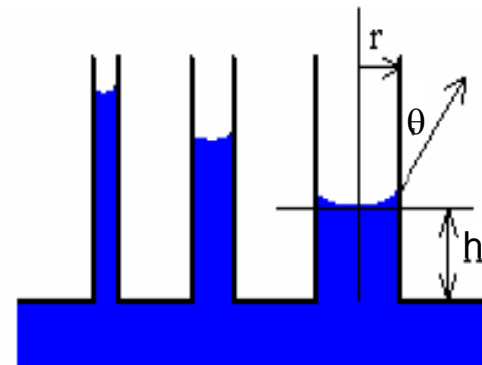
$$d = 10 \text{ mm} \rightarrow h = 3 \text{ mm}$$

$$d = 1 \text{ mm} \rightarrow h = 30 \text{ mm}$$

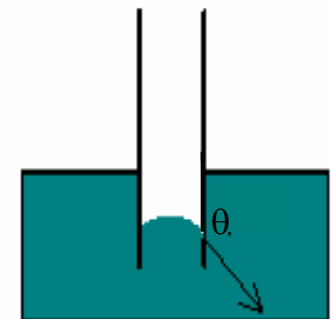
$$d = 100 \text{ } \mu\text{m} \rightarrow h = 300 \text{ mm}$$

$$d = 10 \text{ } \mu\text{m} \rightarrow h = 3 \text{ m}$$

$$d = 1 \text{ } \mu\text{m} \rightarrow h = 30 \text{ m}$$



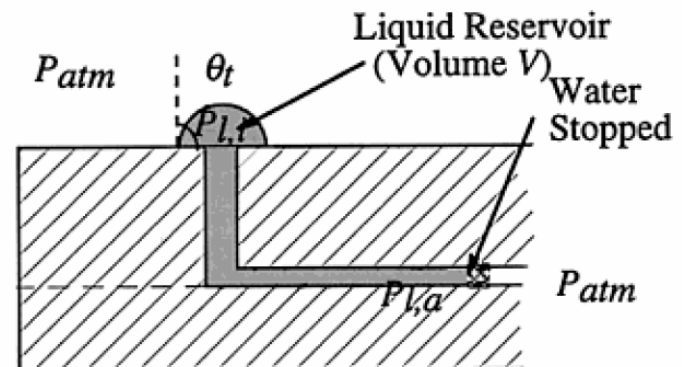
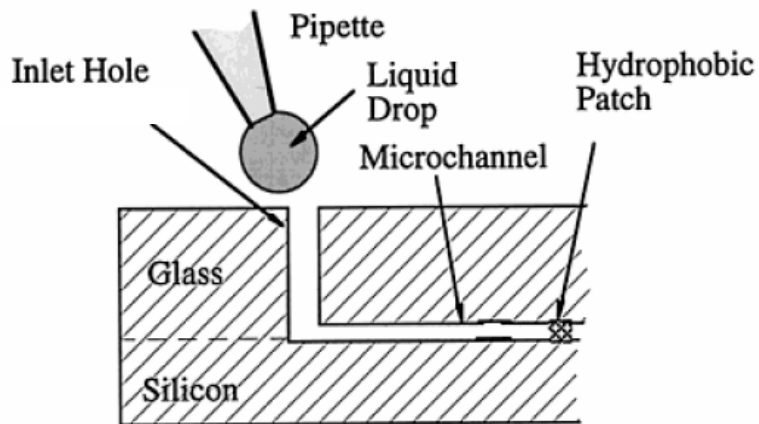
Wetting surface
 $\theta < 90^\circ$



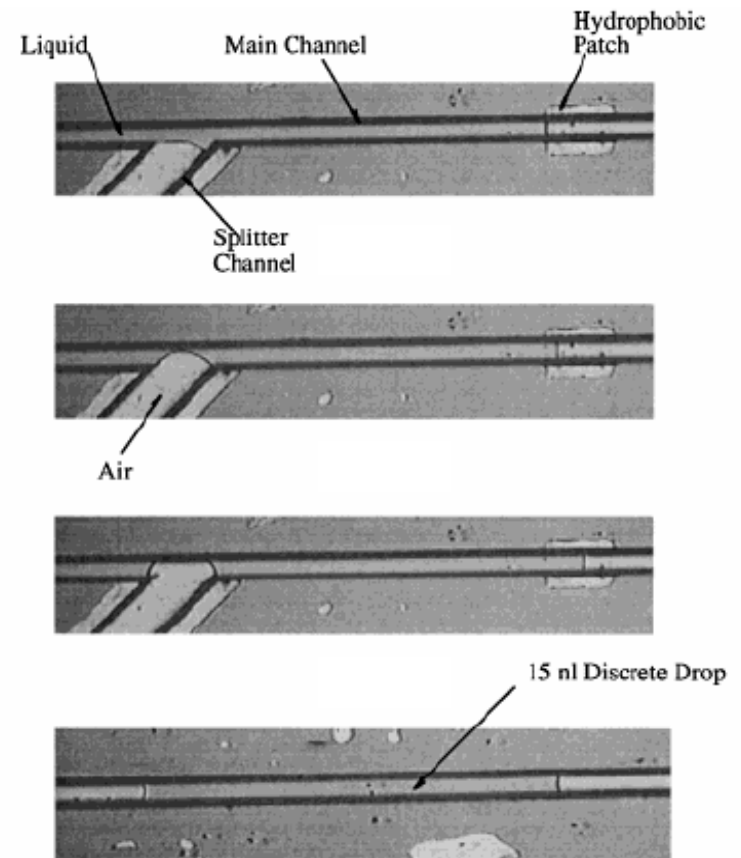
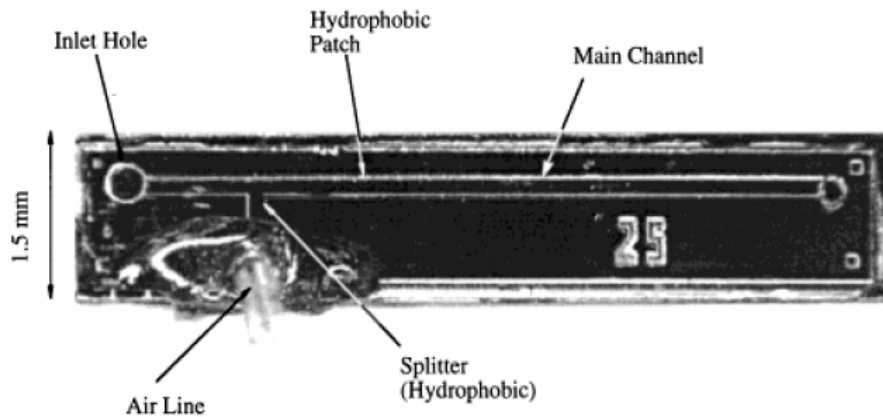
Hydrophobic surface
 $\theta > 90^\circ$

Surface tension

- Surface tension can sometimes be used to advantage:
- Self-filling microfluidic devices
- Nanoliter liquid metering in microchannels using hydrophobic patches

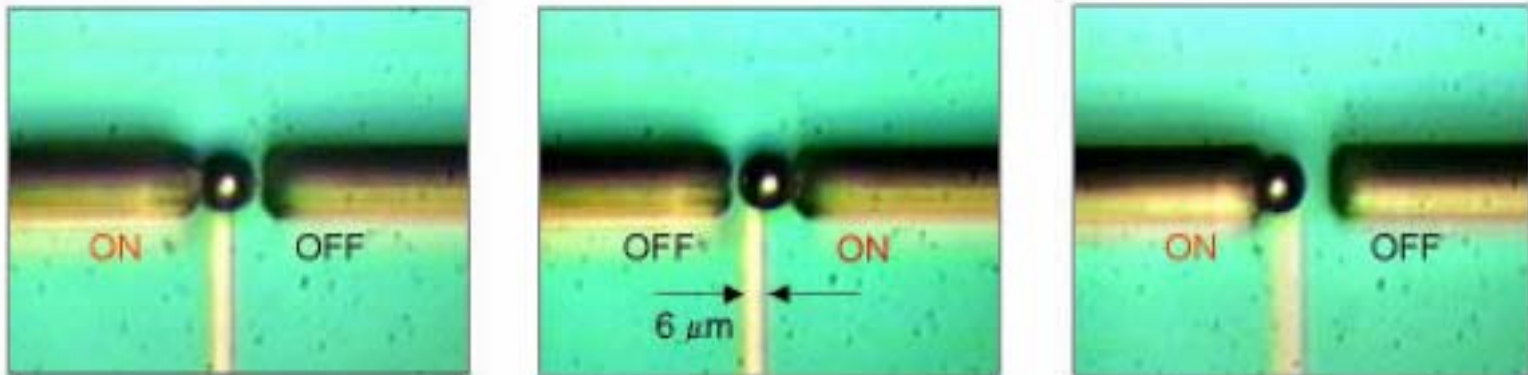


Nanoliter liquid metering in micro-channels



Droplet based micro-switch

Stability of droplets can be exploited: figure shows a liquid mercury droplet manipulated by electrostatic attraction to act as a switch.

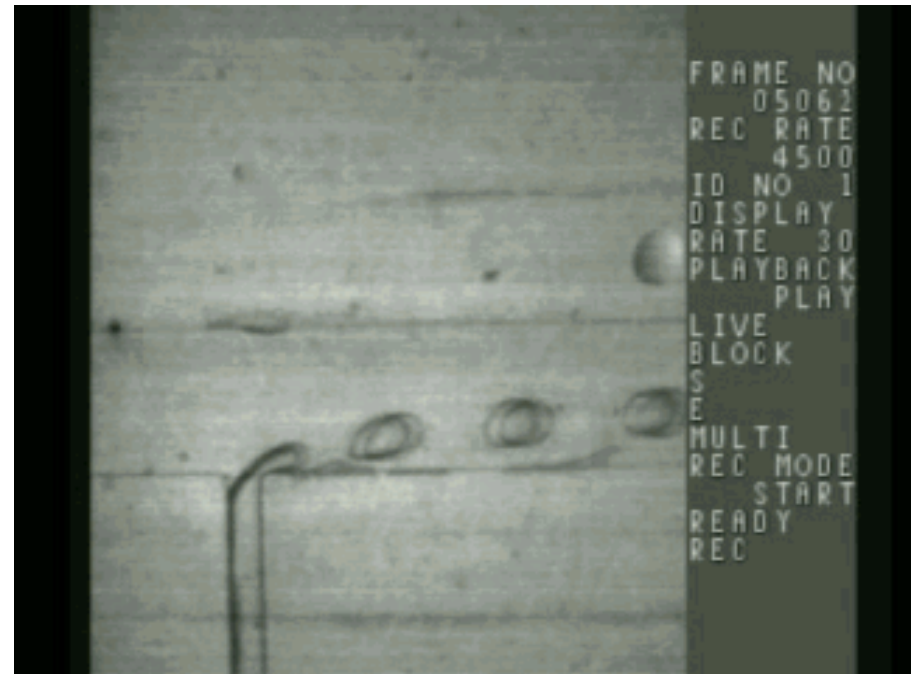


Micro-switch with a droplet of liquid metal (switching at 70V)

Source: C. J. Kim

Droplet-based microfluidics

- Two-phase fluidics may provide a convenient method of transporting individual samples or reaction volumes through a microfluidic device.
- Recent work in Japan and UMIST/DL has demonstrated the production of aqueous droplets within a non-aqueous medium, such as silicone oil.
- The potential advantages are that each droplet represents a transportable individual reaction volume, which is designed not to exchange material with its surroundings.
- Other preliminary results have included the manipulation of droplets in a micro-array, chemical detection within a micro-droplet and electrostatic generation of droplets.

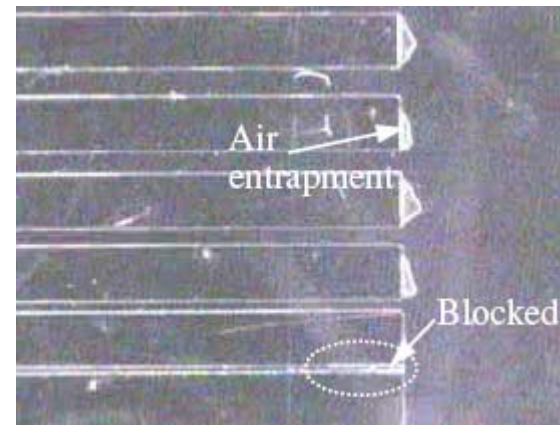
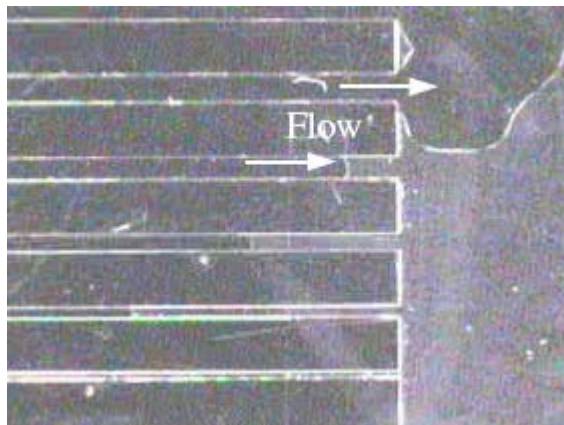


Pressure-driven droplet generation from a 100 μm side channel

Ref: T. Taniguchi, T. Torii and T. Higuchi, *Lab Chip*, 2 (2002) pp. 19-23.

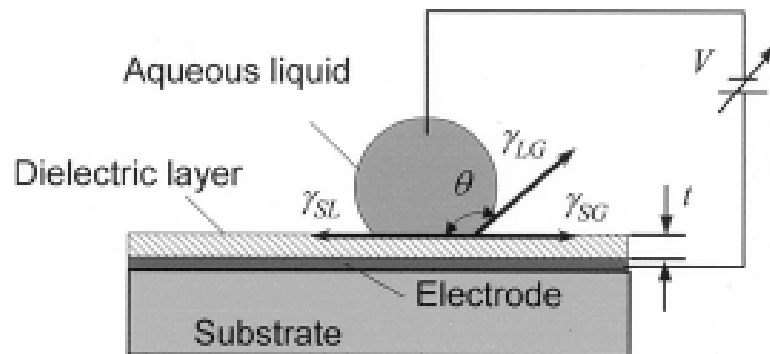
Surface tension

- However, surface tension can create problems with air entrapment



Application Example: Electro-Wetting On Dielectric (EWOD)

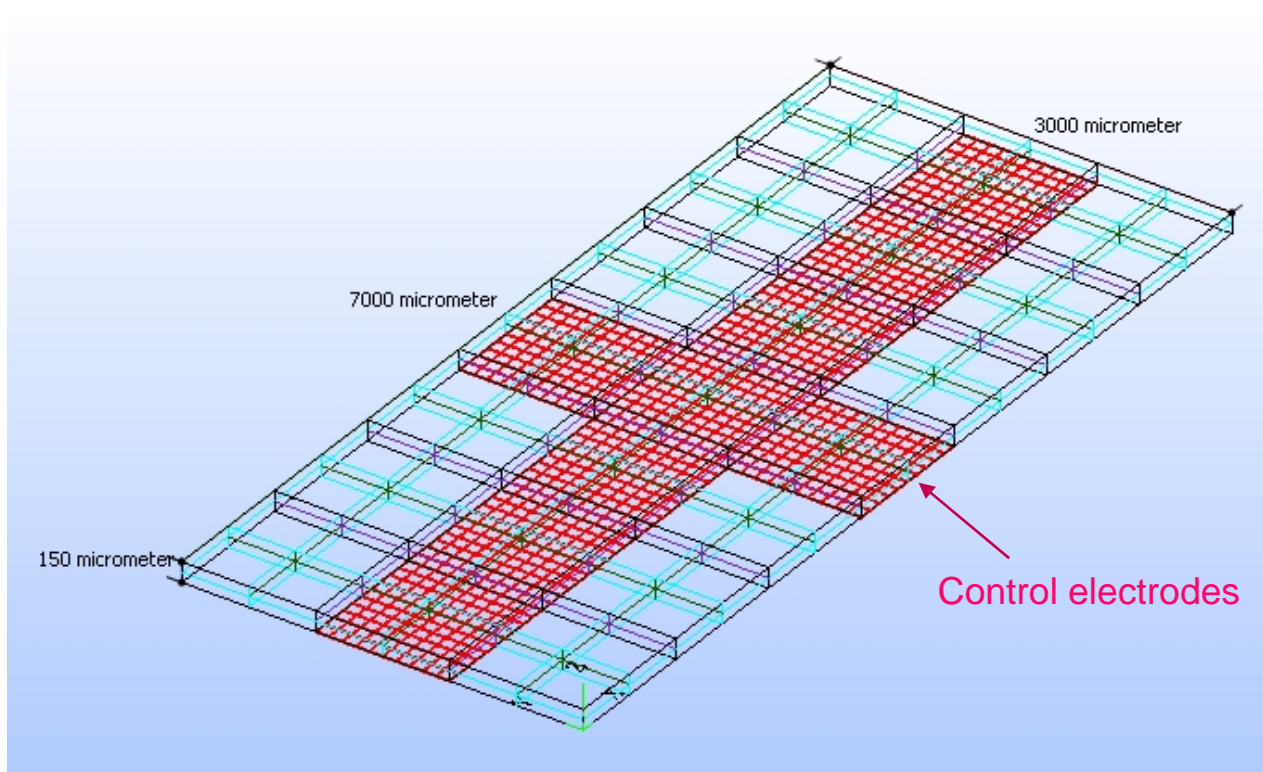
- What is EWOD?
 - This is a technique that allows the user to control the surface tension by the application of a voltage
 - The governing equation was derived by Lippmann (1875)



$$\cos \theta(V) = \cos \theta_Y + \frac{\epsilon_0 \epsilon_t}{2t\gamma_{LG}} V^2$$

- EWOD can be used to move droplets, split droplets or merge droplets
see Cho et al. JMEMS V12 (2003) pp. 70-80.

CFD simulations of droplet transport and splitting using the VOF (volume-of-fluid) module within CFD-ACE+



Computational domain

Computational domain
composed of 7x3 individual
electrodes each
1mm x 1mm square

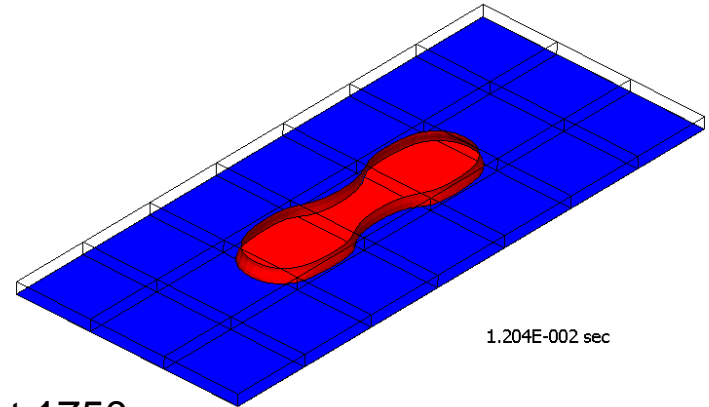
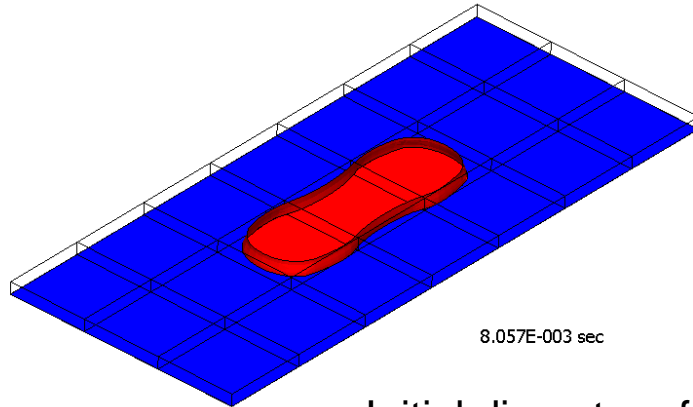
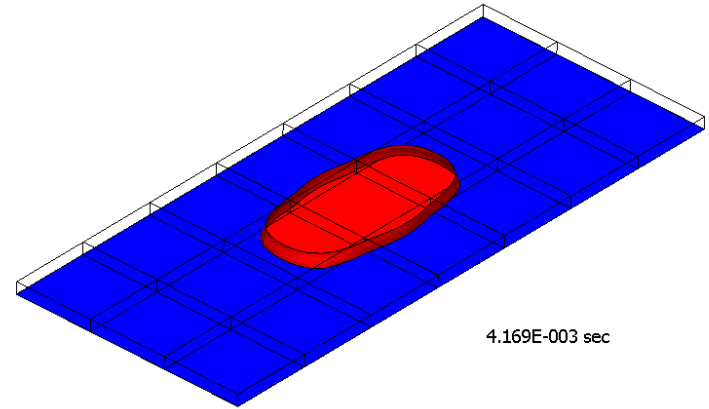
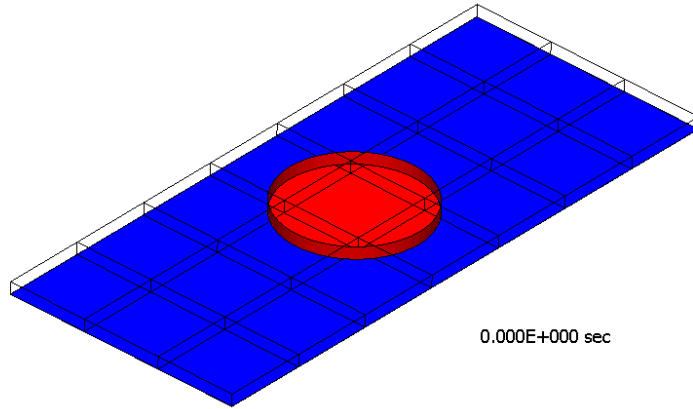
Channel height = 150 μm

3D grid consists of 70x30x8
cells

Change in contact angle over
the control electrodes
calculated using the EWOD
equation:

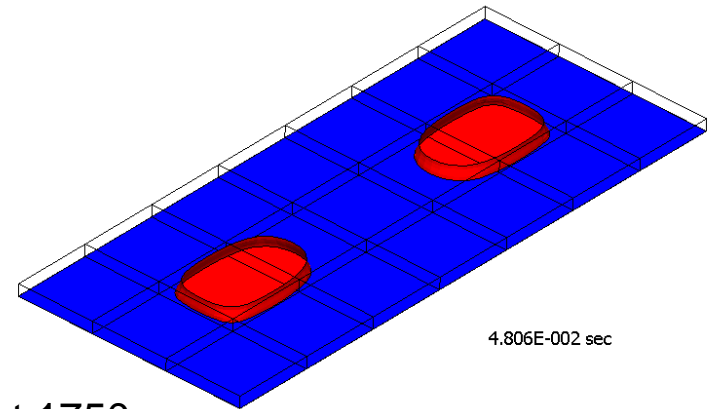
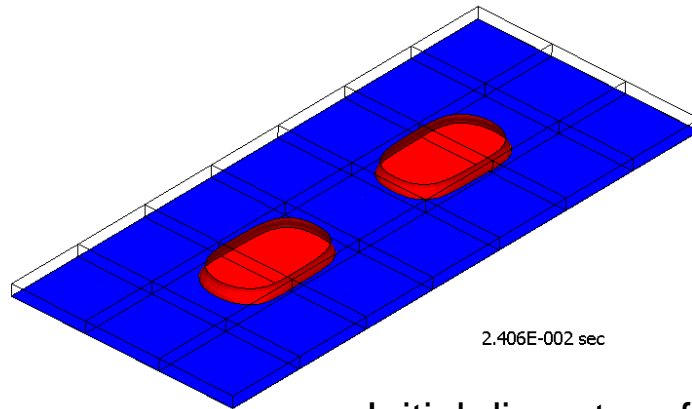
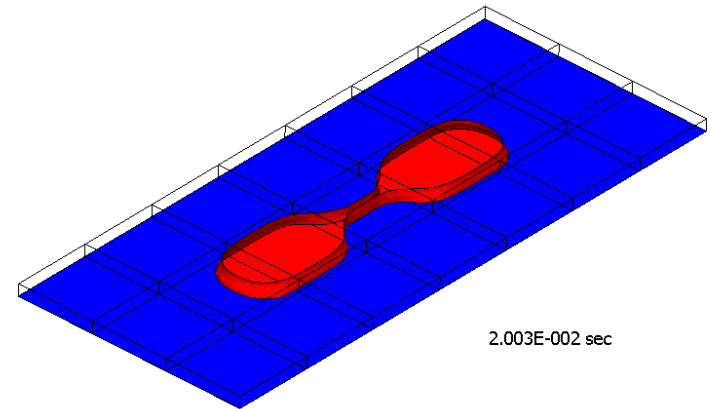
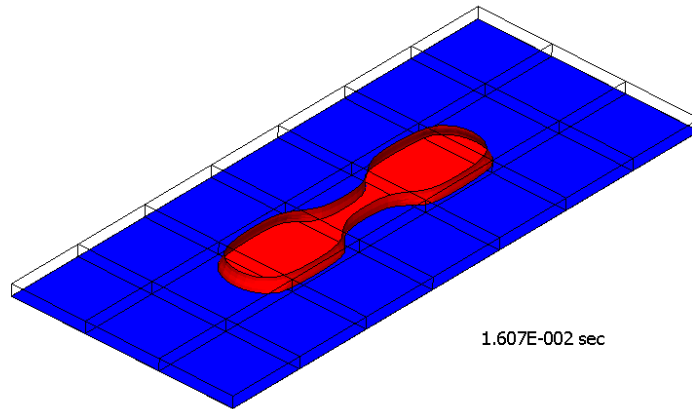
$$\cos \theta = \cos \theta_Y + \frac{\epsilon_0 \epsilon_d}{2d \sigma_{lv}} V^2$$

Simulation of droplet splitting



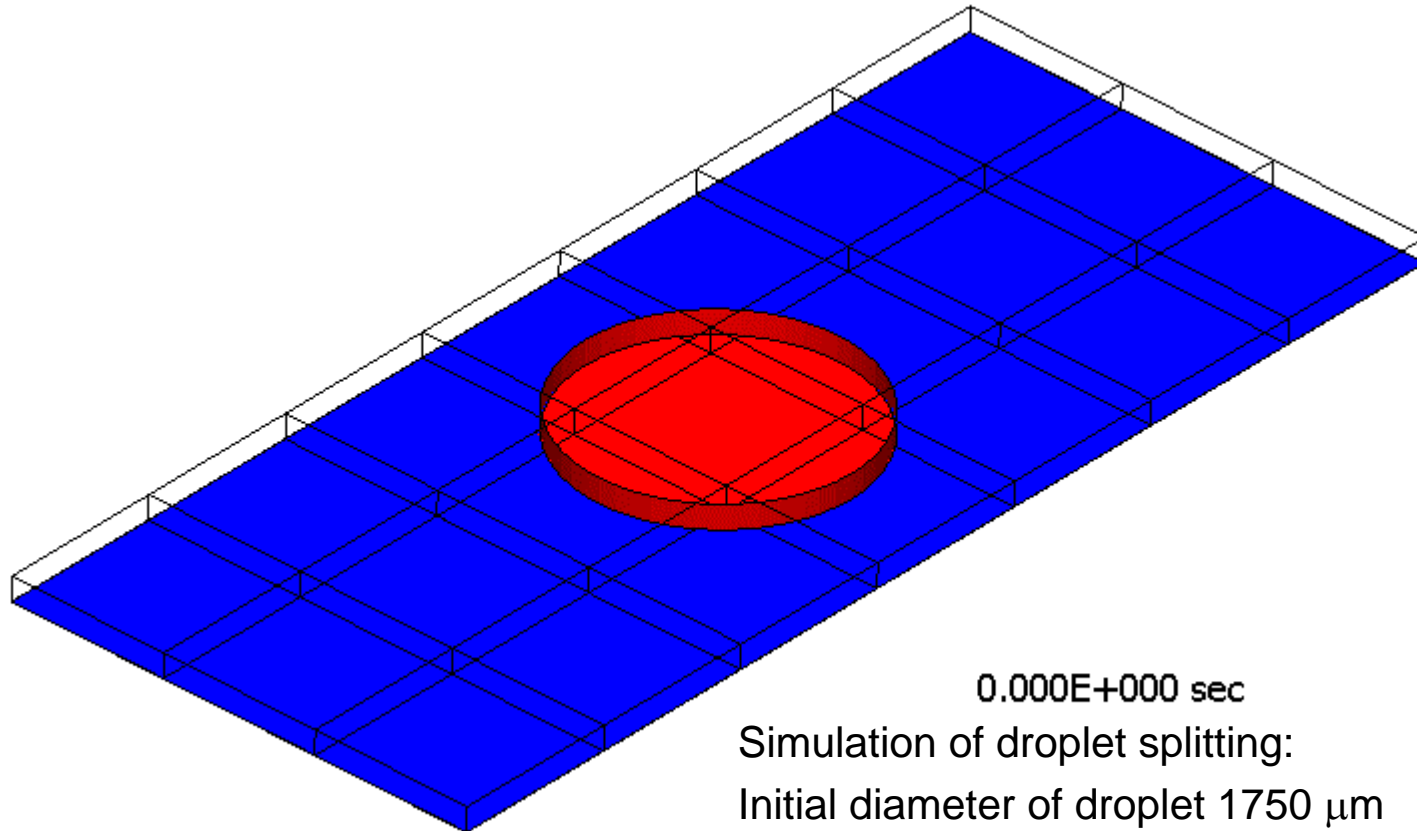
Initial diameter of droplet 1750 μm
75 V applied to control electrodes

Simulation of droplet splitting



Initial diameter of droplet 1750 μm
75 V applied to control electrodes

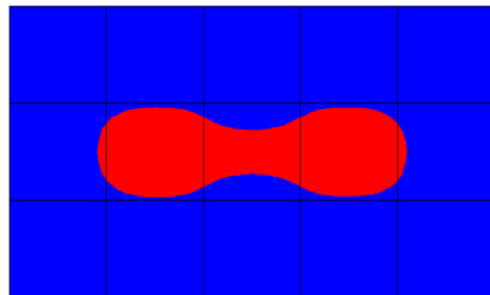
Simulation of droplet splitting



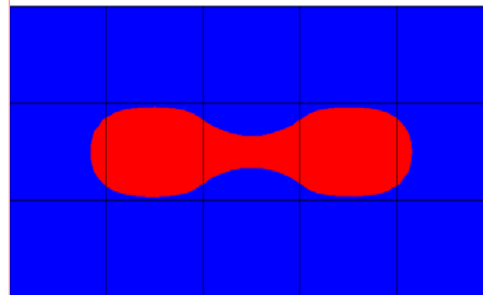
0.000E+000 sec

Simulation of droplet splitting:
Initial diameter of droplet 1750 μm
75 V applied to control electrodes

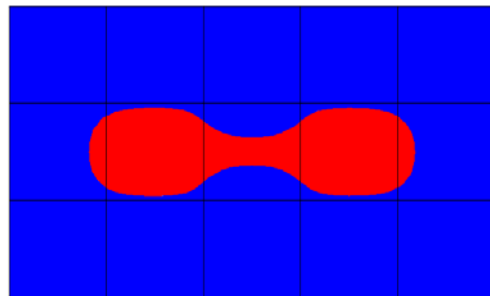
Simulation of droplet splitting



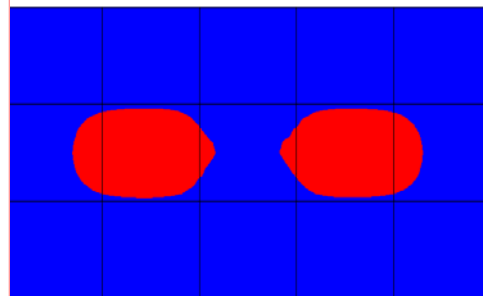
50 V



55 V



60 V



65 V

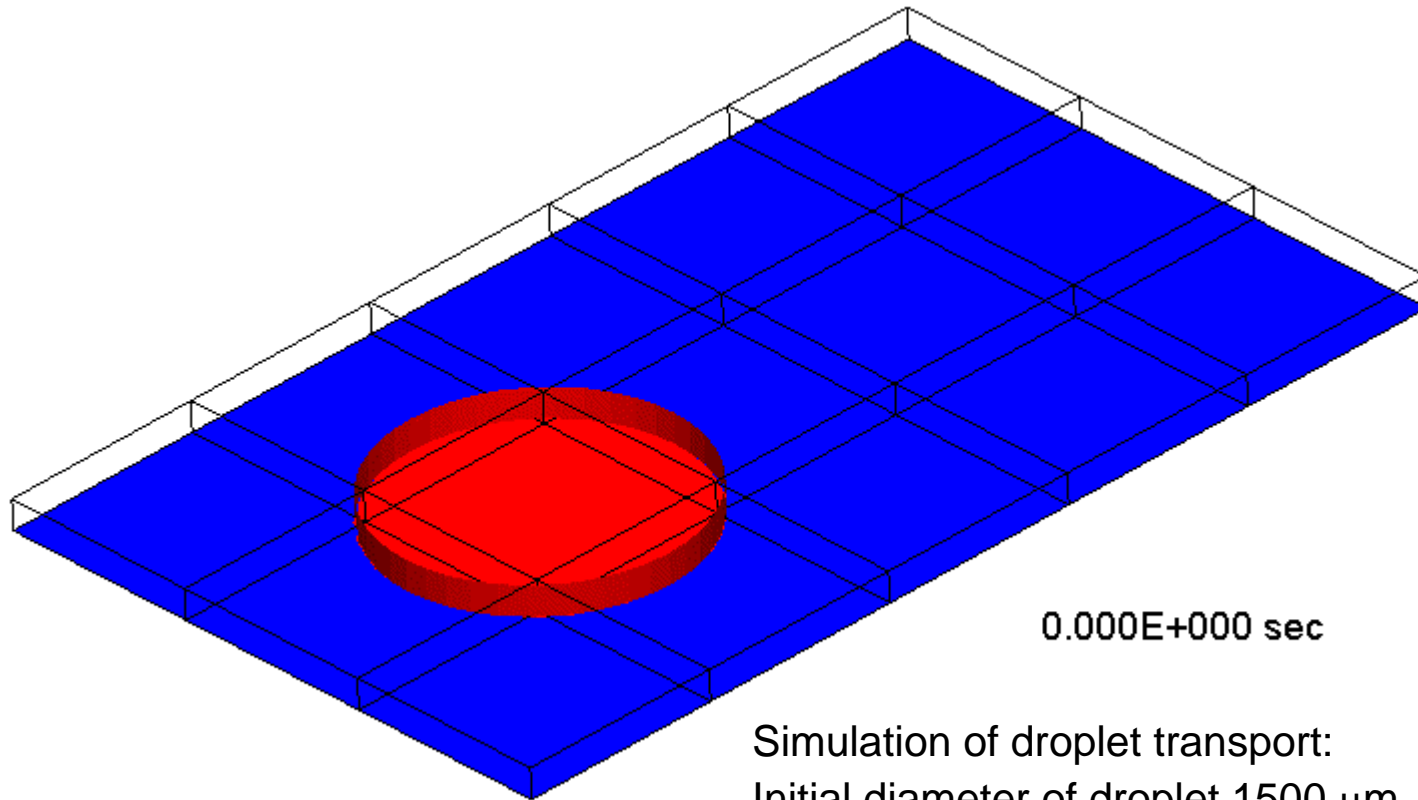
Maximum elongation of droplets as a function
of applied voltage

The simulations have been able to identify a *critical voltage* for the occurrence of droplet splitting

Below the threshold, the droplets fail to split, as shown in the first three cases

The CFD simulations indicate that above 65 V, droplet splitting will occur

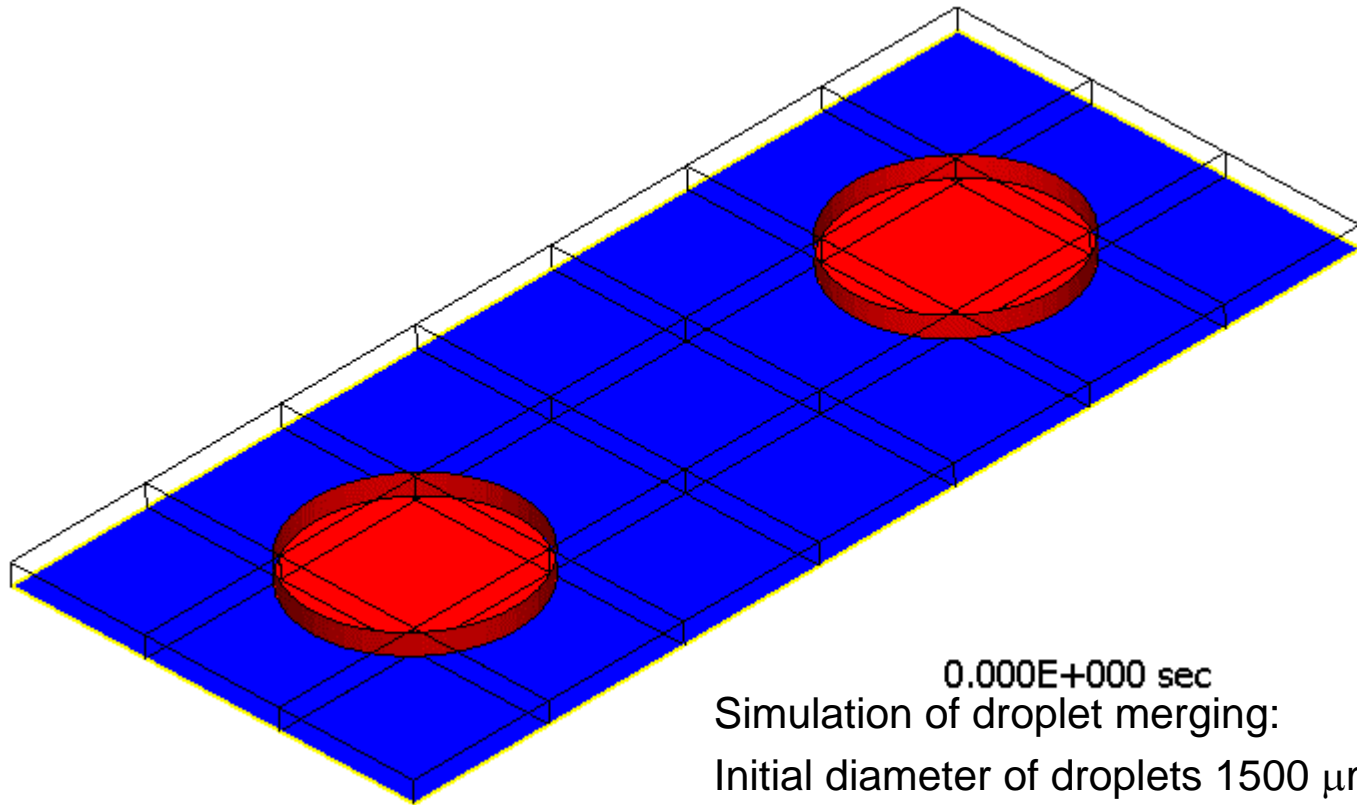
Simulation of droplet motion



0.000E+000 sec

Simulation of droplet transport:
Initial diameter of droplet 1500 μm
50 V applied sequentially to control electrodes

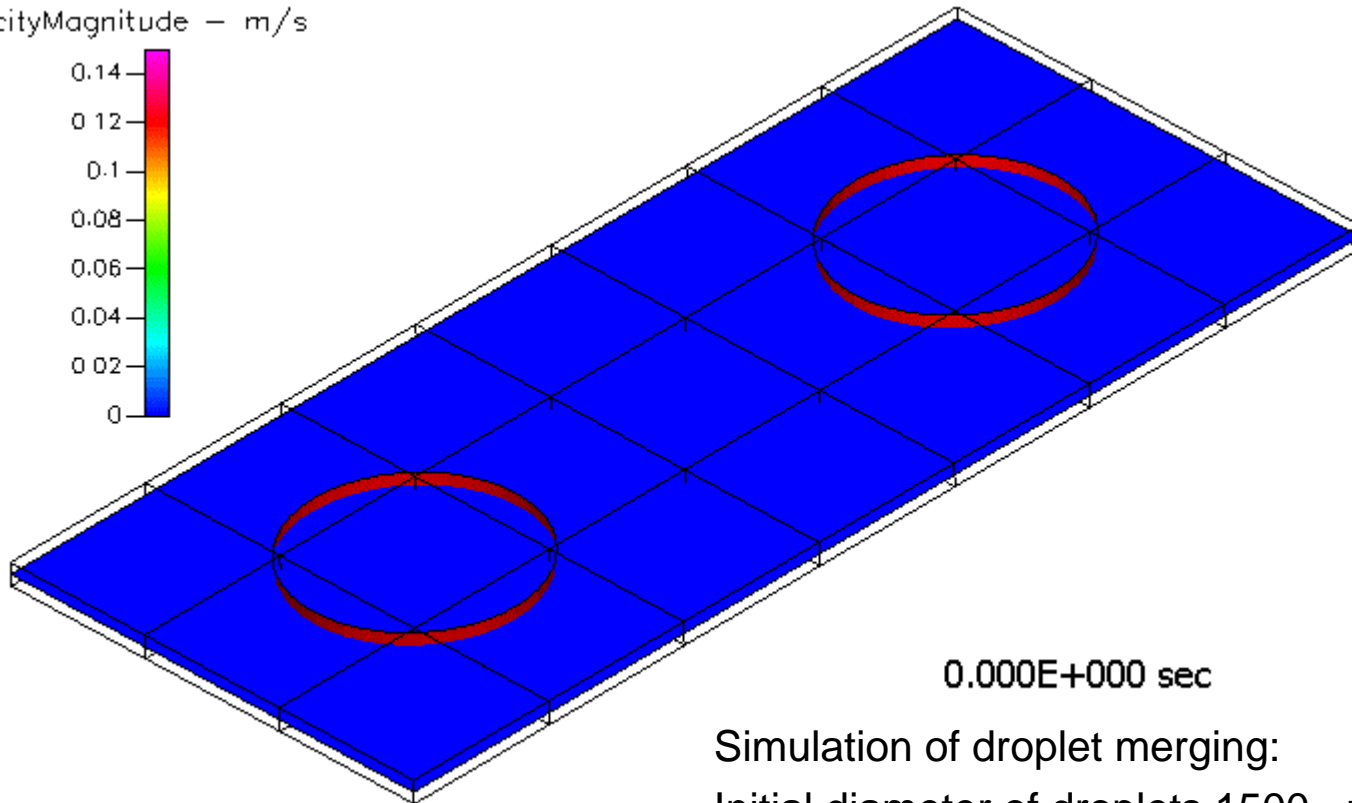
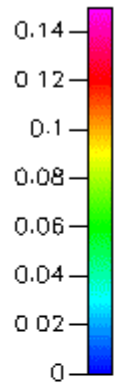
Simulation of droplet merging



0.000E+000 sec
Simulation of droplet merging:
Initial diameter of droplets 1500 μm
50 V applied to control electrodes

Simulation of droplet merging – velocity vectors

VelocityMagnitude – m/s



0.000E+000 sec

Simulation of droplet merging:
Initial diameter of droplets 1500 μm
50 V applied to control electrodes

Microfluidic networks using biologically inspired principles

Outline of topic

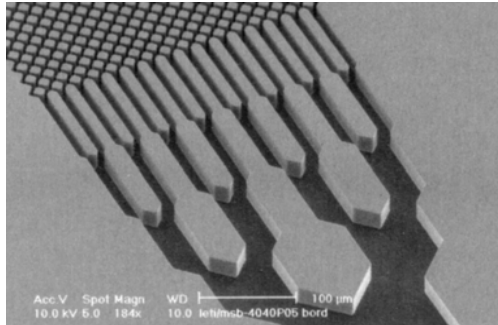
- Examples of hierarchical microfluidic systems
- Organisation of vascular systems in Nature
- **Theoretical basis of Murray's law**
- Generalisation of Murray's law – introduction of a branching parameter, X
- Consequences of Murray's law on the flow behaviour in vascular systems
- **Extension of Murray's law to constant-depth rectangular and trapezoidal channels**
- Further generalisation
- Validation of generalised biomimetic design rule using CFD
- Conclusions

Biomimetics

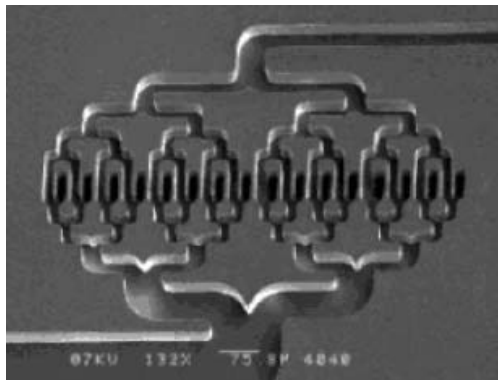
- Nature has always been an abundant source of inspiration. From the earliest of times, Man has sought to replicate or copy ideas that have evolved naturally in plants and animals e.g. the myth of Daedalus and Icarus escaping from Crete by building wings to fly away.
- What is biomimetics?
 - Biomimetics involves using Nature as the inspiration for new designs
 - One example is the Stenocara beetle which “harvests” water in the Namibia desert. This model is now being explored as a way of harvesting fog.



Examples of hierarchical microfluidic systems



BiMEMS structure developed by the CEA-Leti BioChipLab project



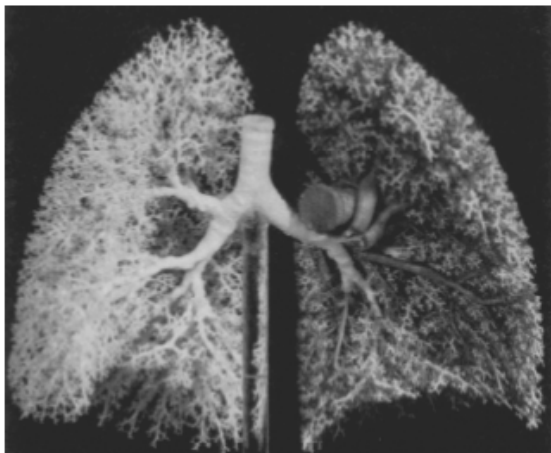
Multi-laminated micromixer developed by Bessoth *et al.* (1999)



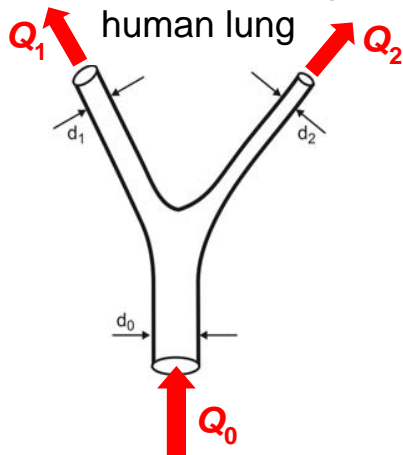
Eight generation multi-width and multi-depth microvasculature fabricated by Lim *et al.* (2003)

- Some microfluidic devices resemble the hierarchical fluid distribution systems found in Nature
- **Biologically-inspired principles could have an important role to play in the design of future lab-on-a-chip systems**

Organisation of vascular systems in Nature



Dichotomous branching in the human lung



Typical bifurcation

- The most distinctive feature of natural (biological) distribution systems is their **hierarchical** or **fractal-like structure** and the successive division of vessels which become smaller both in length and diameter
- The relationship between the diameter of the parent and daughter vessels in mammalian cardiovascular and respiratory systems was first derived by Murray (1926) using the **principle of minimum work**
- Murray found that

$$d_0^3 = d_1^3 + d_2^3$$
- i.e. “*the cube of the diameter of the parent vessel equals the sum of the cubes of the diameters of the daughter vessels*”

Generalisation of Murray's law

$$d_0^3 = 2d_1^3$$

- For a symmetric bifurcation (with $d_1=d_2$), Murray's law reduces to
- Cieřlicki (1999) has shown that Murray's law can be generalised by defining a **branching parameter, X** , which controls the change in diameter at each consecutive generation:

$$X = \frac{d_0^3}{2d_1^3}$$

- For $X = 1$, the parent/daughter branches obey Murray's original hypothesis
- However, X does not necessarily have to be unity, although the resulting system will no longer obey the principle of minimum work
- As will be shown later, the generalised case of $X \neq 1$ can be used to design artificial microfluidic manifolds with very specific (and potentially useful) flow properties

Implications of Murray's law – shear stress

- The shear stress acting on the wall of a circular pipe in a fully-developed laminar flow can be written as

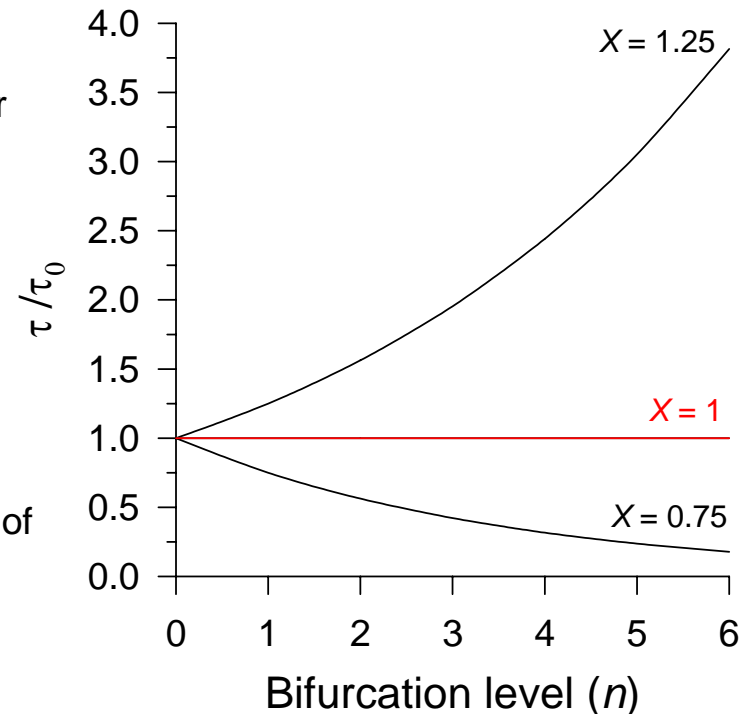
$$\tau = \frac{8\mu\bar{U}}{d}$$

- Substituting for the mean flow velocity and diameter leads to the important relationship:

$$\tau_n = \tau_0 X^n$$

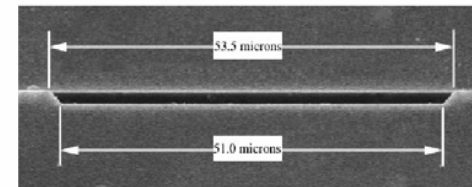
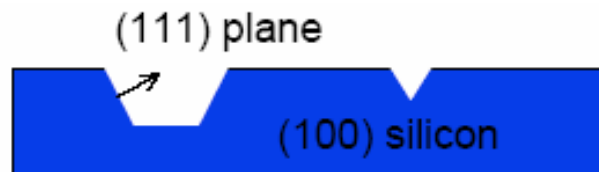
- The wall shear stress remains constant throughout the system when Murray's law is obeyed ($X = 1$)
- However, by changing the value of the branching parameter, X , it is possible to introduce an element of control into the shear stress distribution

Normalised wall shear stress as a function of bifurcation level, n



Extension of Murray's law to non-circular ducts

- Murray's law was originally derived for biological systems where all the vessels have a circular cross-section
- However, the microfabrication processes involved in manufacturing microfluidic devices lead to very distinctive non-circular cross-sections, e.g.
 - Deep reactive ion etching (DRIE) of silicon leads to rectangular channels
 - Anisotropic etching a $\langle 100 \rangle$ silicon wafer with KOH leads to trapezoidal channels having an angle of 54.74° to the $\langle 100 \rangle$ crystalline plane



- A common feature in the fabrication of lab-on-a-chip systems is that the channel depth often remains constant throughout the device
- It is therefore necessary to extend Murray's law so that it can be applied to the non-circular, constant-depth channels found in microfluidic applications

Extending Murray's law to non-circular ducts

- Recall: the wall shear stress distribution predicted by Murray's law can be written as

$$\tau_n = \tau_0 X^n$$

- The extension of Murray's law to non-circular ducts can be achieved using an analogous equation but based on the mean tangential shear stress around the cross-section, i.e.

$$\bar{\tau}_n = \bar{\tau}_0 X^n \quad (\text{A})$$

- The mean wall shear stress can be related to the **Fanning friction factor, f** , which in turn can be expressed in terms of the *Poiseuille number*, Po and *Reynolds number*, Re

$$\bar{\tau} = \frac{1}{2} \rho \bar{U}^2 f = \frac{1}{2} \rho \bar{U}^2 \frac{Po}{Re} = \frac{\mu \bar{U} Po}{2 D_h} \quad (\text{B})$$

where D_h is the hydraulic diameter = 4 x area / wetted perimeter

- Substituting eqn. (B) into (A) yields a generalised biomimetic design rule that can be applied to all channel shapes irrespective of the cross-sectional geometry:

Generalised biomimetic design rule based on shear stress

$$\frac{\bar{U}_n Po_n}{D_{hn}} = \frac{\bar{U}_0 Po_0}{D_{h0}} X^n$$

The only practical limitation of this eqn. is the requirement to know the hydraulic diameter and the Poiseuille number

Application to a constant-depth **rectangular** manifold

- We define the aspect ratio of the n^{th} generation as $\alpha_n = d / w_n$
- After some algebraic manipulation, it can be shown that the generalised biomimetic design rule can be written as a function of the aspect ratio, α_n

$$\alpha_n (1 + \alpha_n) \text{Po}(\alpha_n^*) = (2X)^n \alpha_0 (1 + \alpha_0) \text{Po}(\alpha_0^*) \quad (\text{C})$$

- The Poiseuille number for a rectangular cross-section can be determined analytically:

$$\text{Po}(\alpha_n^*) = 24 \left[1 - \frac{192}{\pi^5} \frac{1}{\alpha_n^*} \sum_{i=1,3,5,\dots}^{\infty} \frac{1}{i^5} \tanh\left(\frac{i\pi\alpha_n^*}{2}\right) \right]^{-1} \left(1 + \frac{1}{\alpha_n^*} \right)^{-2}$$

Application to a constant-depth **trapezoidal** manifold

- Using a similar technique, the aspect ratio of a trapezoidal channel can be defined as $\gamma = d / a$ where a is the widest channel dimension
- After some algebraic manipulation, it can be shown that the generalised biomimetic design rule can again be written as a function of the channel aspect ratio:

$$\frac{\sqrt{2}\gamma_n + (\sqrt{3} - 1)\gamma_n^2}{(\sqrt{2} - \gamma_n)^2} \text{Po}(\gamma_n) = (2X)^n \frac{\sqrt{2}\gamma_0 + (\sqrt{3} - 1)\gamma_0^2}{(\sqrt{2} - \gamma_0)^2} \text{Po}(\gamma_0)$$

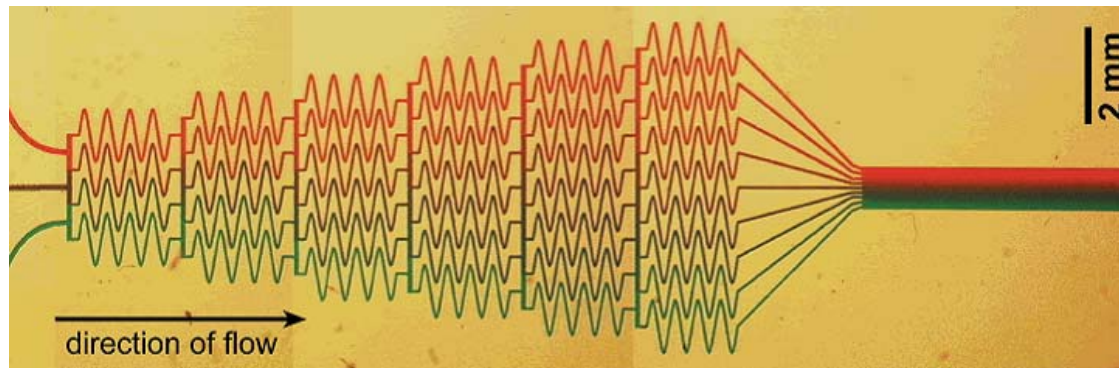
- The Poiseuille number for a trapezoidal channel cannot be obtained analytically. However, Morini (2004) has shown that the Poiseuille number for KOH-etched <100> silicon channels can be determined from a 5th order polynomial as follows

$$\text{Po}(\gamma_n) = 24 \left[1 - b_1\gamma_n + b_2\gamma_n^2 - b_3\gamma_n^3 + b_4\gamma_n^4 - b_5\gamma_n^5 \right]$$

where the coefficients have the values of $b_1=1.7611$, $b_2=2.6780$, $b_3=4.9342$, $b_4=10.0883$ and $b_5=7.4496$

Biomimetic design rule for other microfluidic manifolds

- The proposed biomimetic design rule based on shear stress can also be adapted to other designs of microfluidic manifold
- For example, it is possible to generate linear concentration gradients by recombining the output from a hierarchical mixer where the number of channels increases by one each generation:-



Example of a 3-inlet/9-outlet microfluidic manifold developed by Dertinger *et al.* (2001) for generating linear concentration gradients (Analytical Chemistry, 2001, 73, p. 1242).

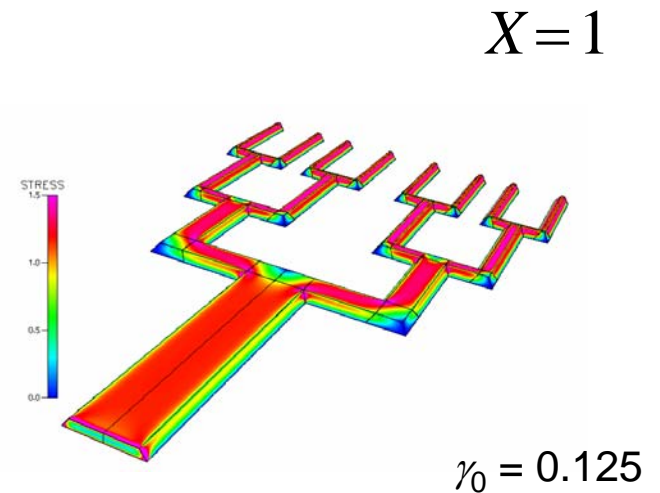
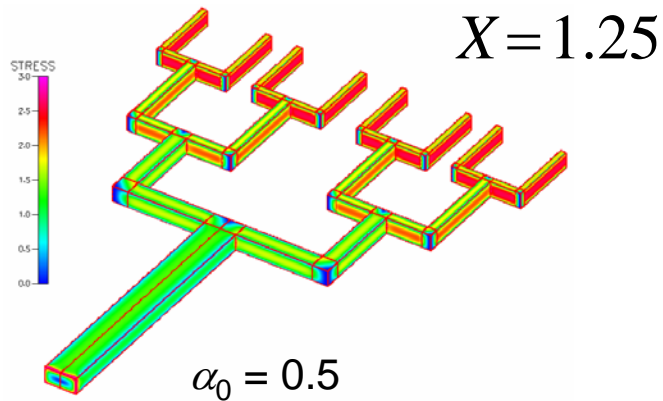
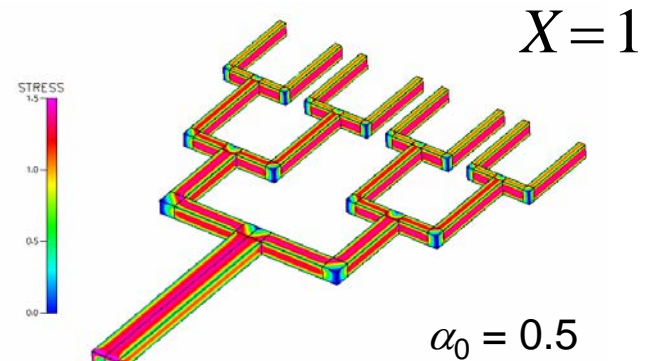
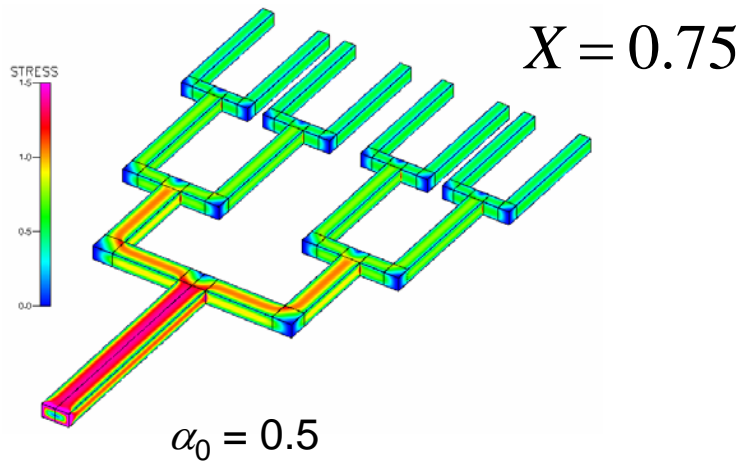
- The mixer fabricated by Dertinger *et al.* employed constant cross-section channels rather than following a strict biomimetic principle
- It is informative, however, to consider how the present biomimetic approach could be used to redesign the channel dimensions according to biologically inspired principles

Validation of biomimetic design rules

Validation against CFD simulations

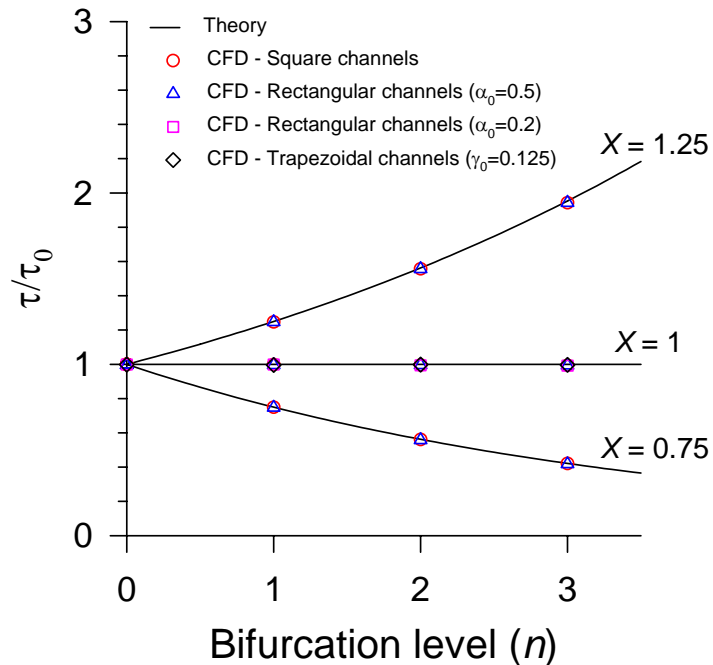
- A comprehensive series of computational fluid dynamics (CFD) simulations were performed to assess the applicability of the proposed biomimetic design rule and demonstrate how Murray's law can be applied to the design of non-circular microfluidic manifolds
- The simulations considered a series of branching microfluidic networks composed of **multi-depth square channels** and **constant-depth rectangular and trapezoidal channels**
- The manifolds were restricted to four generations ($n = 0, 1, 2, 3$) and each followed the strict biomimetic principle that the length of each flow segment is proportional to its hydraulic diameter
- The numerical simulations were conducted using the commercial computational fluid dynamics software package, CFD-ACE+ (ESI CFD, Huntsville, USA). The meshes representing the networks contained between 1 and 2.4 million grid nodes depending upon the geometry and the value of X

Predicted normalised wall shear stress distributions

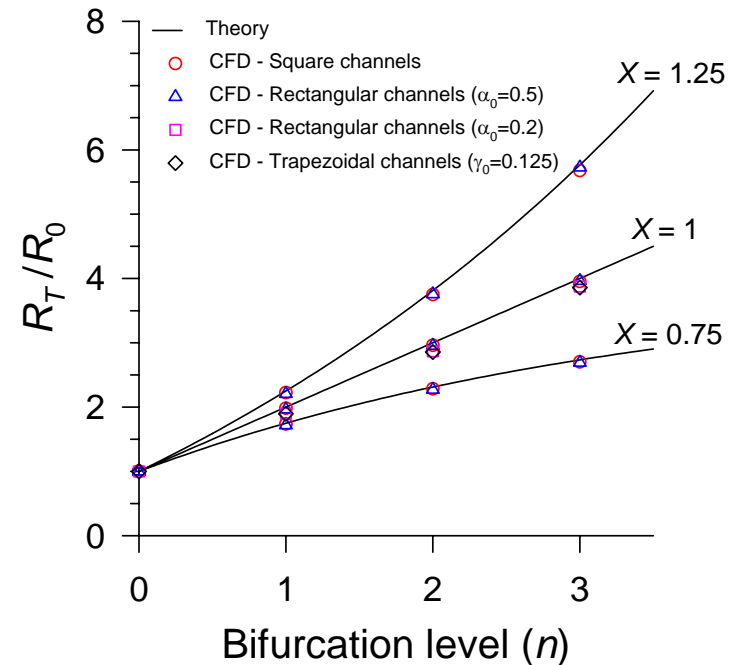


Comparison between CFD and theoretical results

Normalised mean wall shear stress as a function of bifurcation level, n



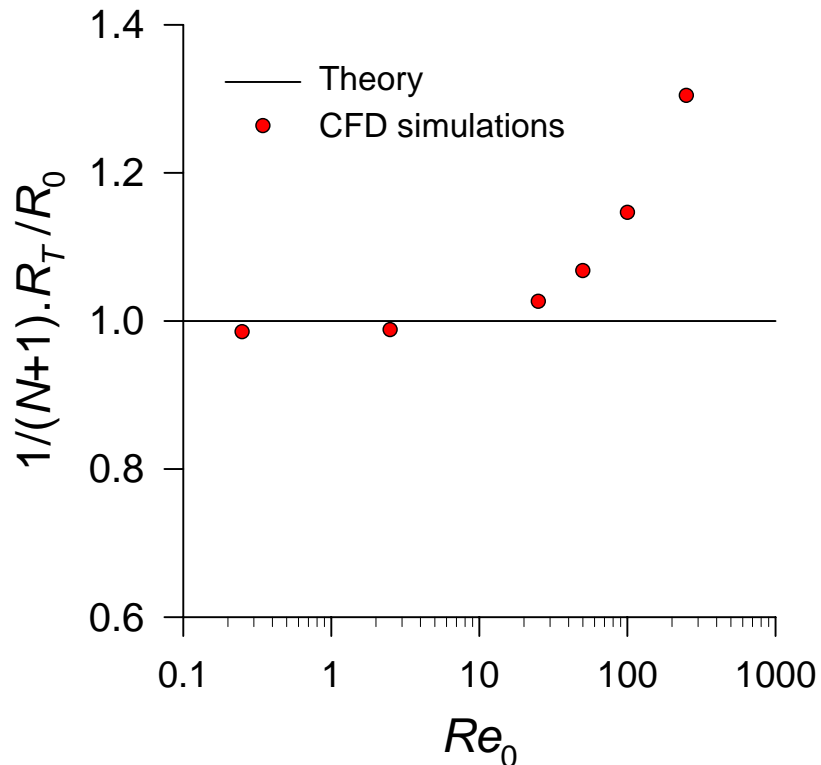
Normalised total flow resistance as a function of bifurcation level, n



- The numerical predictions are in very good agreement with the theory, demonstrating the applicability of the proposed biomimetic design principle
- The shear stress and resistance distributions demonstrate that the flow characteristics are unaffected by the shape or aspect ratio of the channels

Comparison between CFD and theoretical results

Normalised flow resistance $1/(N+1) \times R_T / R_0$
as a function of bifurcation level, n



- The theoretical description assumes the flow is laminar and fully-developed
- However, the theory does not take account of the pressure losses associated with the T-junctions and 90° bends found in the example used
- For $Re_0 \leq 25$, the error in the predicted flow resistance is less than 2%
- For $Re_0 = 50$, the theory underpredicts the CFD results by approximately 6% and this error grows to around 30% at $Re_0 = 250$
- The pressure losses can be attributed to the formation of secondary eddies at each bend

First Latin American SCAT Workshop:
Advanced Scientific Computing and Applications

Mixing, Droplets, Biomimetics, . .

Prof David Emerson
CCLRC Daresbury Laboratory
University of Strathclyde

